CHAPTER 3

ANALYTICAL MODEL

3.1 Girder End Movement

It is necessary to determine end movements of simply supported girders by means of axial deformation, end rotation and end translation in provision structures separated by expansion joints and provision deck continuity by eliminating gaps and joints between adjacent spans for smooth riding, noise reduction and service improvement as well. In this part the stress, strain and deformations of a member for the elongations or end rotation are not restrained by the supports or by continuity with other members. From the section analysis, the results of axial strain and curvature in each section through the girder's length can be determined and can be converted to end movements of highway girders by principle of virtual work. In addition, the end translation is related to the vertical stiffness of elastomeric bearing and moving load.

The end movements can be separated into two parts as short-term and long-term movements. Traffic loads, temperature gradients and ambient temperatures are considered in short-term movement. Creep, shrinkage of concrete and relaxation of prestressing steel are considered in long-term movement.

In this study, the incremental time steps method with the nonlinearity due to the time dependent deformations is used to determine end movements in the girder model because it is the best analyzed approach to determine both stresses and deformations as shown in chapter 2. These end movements are determined in order to compare the amount of end movements due to the effect of each variable. The comparison between short-term and long-term deflection is directly dependant on the shape of creep, shrinkage and steel relaxation models. The end movements that are used in link slabs are taken from deck casting time because the link slab can ensure that these movements are restrained after the hardening of concrete in the link slab. In the analysis, the typical girders which are I, T, U and Box-sections with different span length ranged from 21 to 45 meters are considered as the samples of this study as shown in Table 3.1.

Because the long-term deflection is dependant on creep, shrinkage and steel relaxation, it is also dependant on the variables of these models which are the type of concrete, concrete strength, volume-to-surface ratio (V/S), relative humidity and construction time following ACI and CEB-FIP codes including the section properties and prestressing force. The assumed constants and variables of construction time are shown in Table 3.2.

Figure 3.1 shows the creep coefficient and shrinkage strain comparison between ACI (1992), CEB-FIP (1990) codes and test result of Thailand-based specimens (Institut Fuer Stahlbeton- und Massivbau, Universitaet Innsbruck, 1986) including relaxation of low-relaxation strand or prestressing bars (OHBDC, 1983). The end movements occur at neutral axis of main girder so the girder height and the support level are not considered in this model but they will be considered in the interaction model.

The results of axial deformation and end rotation from the deck casting time of precast member and composite member due to long-term effects followed CEB-FIP varied with construction time are shown in Figs. 3.2 – 3.3. The age of the precast member at the release of prestressing force has more influence on end movements than the age of the precast member at the casting of deck slab due to creep, shrinkage and steel relaxation because the properties of concrete at the early age experience more change.

The long-term axial deformation is shortening due to creep and shrinkage but is elongating due to steel relaxation. In addition, the long-term end movement is camber (upward) due to creep but is deflected (downward) due to different shrinkage and steel relaxation. The creep and steel relaxation affect both axial deformation and end rotation related to axial strain (P/EA) and curvature (M/EI) respectively but in different direction of movements. Shrinkage affects axial deformation related to construction time and affects end rotation related to both construction time and sectional dimension. The long-term effects which are due to creep, shrinkage and steel relaxation can be assumed to be related to axial strain (P/EA) and curvature (M/EI).

The incremental time steps method is reasonable as a procedure to determine the correct amount of end movements. The sources of end movements are the creep and shrinkage models as shown in Fig. 3.1 with relaxation of prestressing steel and 25 °C in temperature gradient with ±25 °C in ambient temperature. The end movements

from deck casting time at a 30-day aged precast member due to each effect are shown in Fig. 3.4 with the variation of span length. The axial deformation due to ambient temperature and long-term effects is significantly dependant on span lengths, although the axial deformation due to long- term effects is dependant on the section properties. However, the end rotation due to long-term effects, the axial deformation and end rotation due to temperature gradient and live loads are still dependant on section properties. The maximum shortening axial deformation of girders is caused by long-term effects, a decrease in ambient temperature and the temperature gradient of girders before deck casting. In addition, the maximum elongation axial deformation of girders is caused by live loads, an increase in ambient temperature and the temperature gradient of girders at the time of service. The maximum camber end rotation of highway girders is caused by long-term effects and temperature gradient at service, and its maximum deflected end rotation is caused by live loads and the temperature gradient at the deck casting time. They are shown in Fig. 3.5 and Tables 3.3 – 3.6. So the cases of end movement of highway girders for link slab boundaries should be taken into consideration in all four cases.

The end movements of highway girders are affected by the time-dependent properties of material that act together and the other variables that are construction times and section properties, therefore, the end movements from each source cannot be done by superposition. The simplified prediction method, which operates under some assumptions and is used as a design tool in the PCI Design Handbook (1988), does not concern the shrinkage effect under its assumptions.

3.2 Finite Element Analysis of Link Slab

The purpose of this chapter is to have a closer look at the behavior of link slabs and to reveal the influences on the detailing of reinforcement and the thickness-to-span ratio in link slabs under four independent actions, namely axial deformation, end rotation movement, end vertical movement (translation) and mid-span loading with fix-ended support as shown in Table 3.7. In reality, a link slab is subjected to these boundary conditions almost simultaneously due to interaction between adjacent girders, link slabs and support stiffness. To develop a complete interaction model, one needs to fully understand the link slab behavior under each condition. Pre- and post-

processing of the analysis are performed by a commercial program FEMAP with a finite element code MASA. This code is based on the microplane model.

3.2.1 Modeling of Concrete Material and Reinforcing steel

The concrete material is modeled by using 8-node solid elements. A comparison of concrete behavior using a microplane constitutive law that comes from a stress-strain relationship given by Hognestad (1951) for a uniaxial compression is shown in Fig. 3.6(a). The microplane model implies that Young's modulus, Poisson's ratio and 12 microplane parameters have to be obtained such that the model fits the macroscopic properties of concrete. In the finite element code, the microplane model parameters are automatically generated for a set of given macroscopic concrete properties. It can be seen from Fig. 3.6(a) that the microplane model realistically simulates both pre-peak (hardening) and post-peak (softening) responses of a concrete material.

The constitutive law for reinforcing steel is given by a uniaxial stress-strain law as shown in Fig. 3.6(b). The yielding strength f_y, Young's modulus E, hardening modulus E_h and strength f_s have to be given as the input material parameters for a bar element. It is also assumed that the constitutive laws for reinforcing steel under tension and compression are the same in the model.

The spatial finite element model for a link slab is shown in Fig. 3.7. As mentioned previously, concrete is discretized by using 8-node solid elements and reinforcing steel is modeled with 2-node bar elements. Four boundary conditions are considered in the numerical study, namely axial deformation, end rotation, end translation and mid-span loading. In each case, loading is applied by displacement control with boundary conditions being prescribed as shown in Fig. 3.8 and a link slab is modeled according to the symmetry of the problem. Reinforcing steel and surrounding concrete are assumed to be perfectly bonded in the analysis, i.e. no slip in reinforcement occurs. In addition, both vertical and horizontal loads are applied over an elastic plate, which is discretized by using 8-node solid elements with linear elastic behavior, as shown in Fig. 3.7(b).

Three link slabs with different lengths of lap reinforcement, namely fully continuous (LS_F), semi continuous (LS_S) and mid-span hinge (LS_H), are considered in the numerical study as shown in Fig. 3.9. For a semi continuous slab,

the length of lap reinforcement or loop joint is chosen to be 250 mm. The size of the link slab in numerical examples was selected according to practical constructions in different thickness-to-span ratio (Goris, 1985). The support of the link slab for the mid-span loading case is assumed to be fixed because the stiffness of the girder is much higher than that of the link slab (Zia et al, 1995). In addition, the supports are designed to produce both positive and negative bending moments as well as inflection points in the link slab to study the effect of lap reinforcement detailing on the internal force distributions along the span length of the slab.

3.2.2   Finite Element Solutions

Finite element solutions for load-deflection relationships and crack patterns of all lengths of lap reinforcement for link slabs under axial deformation, end rotation, end translation and mid-span loading are presented in Figs. 3.10 to 3.13 respectively.

Numerical results shown in Fig. 3.10 indicate that the length of lap reinforcement has a significant influence on the crack pattern (crack distribution) and the cracking load of a link slab under axial deformation. In a mid-span hinge slab (LS_H) the first crack, which is also the widest one, is observed at the saw cut. On the other hand, cracks in the other two slabs (LS_S and LS_F) are distributed over the entire slabs. It is also found that the LS_H slab yields the minimum cracking load whereas the cracking loads for LS_S and LS_F slabs are almost the same. After the slab is cracked, the slab stiffness shows a notable dependence on the stiffness of reinforcing bars that have enough development length along the span, as shown in the load-deformation curves in Fig. 3.10(a).

The crack patterns under end rotation in Fig. 3.11 show a similar trend to those observed in the slabs under axial deformation. Cracks in a LS-S slab start from the support end and mid-span sections to the quarter-span, whereas for a LS-F slab, cracks start from the support end to the mid-span sections. In addition, the widest cracks in both slabs are found in the earliest cracks. Similar to what was observed in the axial deformation case, the cracking and ultimate moments of LS_H are lower than those of LS_S and LS_F slabs because of a weak section at the saw cut. After cracking, the slab stiffness once again depends significantly on the lap reinforcement details.

Numerical results shown in Fig. 3.12 indicate that the cracking moment, crack distribution and stiffness of link slabs under end translation show negligible dependence on the length of lap reinforcement since the maximum moment in this case occurs at the support where all types of slabs have the same section properties.

For link slabs with fix-ended supports under mid-span loading in Fig. 3.13, the crack distribution near the support (negative moment cracks) is the same for all reinforcement detailing. However, the cracking pattern near the mid-span of the slabs (positive moment cracks) shows a significant dependence on the length of lap reinforcement. It is found that a LS_F slab has the smallest crack width followed by LS_S and LS_H slabs respectively. Additional results for the mid-span loading case are presented in the next chapter. The numerical results of link slabs under the action of mid-span loading will be verified with the experimental results in the next chapter in the form of crack patterns, crack width, failure modes, stress in reinforcement, and load deflection relationships.

3.2.3 Effective Moment of Inertia of Link Slabs

Under service loading, the section properties of a link slab change from an uncracked section to a fully or severely cracked section since cracks will normally occur in the link slab. Determination of the effective moment of inertia for a link slab is necessary to accurately predict the deflection of the slab and the restraint force from adjacent girders. Branson (1965) presented a well-known expression to compute the average effective moment of inertia for a simply-supported rectangular or T-beam under uniformly distributed loading as follows:

$$I_e = \left(\frac{M_{cr}}{M_a}\right)^m I_g + \left[1 - \left(\frac{M_{cr}}{M_a}\right)^m\right] I_{cr} \tag{3.1}$$

For a fix-ended beam, the above equation becomes:

$$I_e = 0.70 I_m + 0.15\left(I_{e1} + I_{e2}\right) \tag{3.2}$$

where I_{cr} and I_g are the moment of inertia of the completed cracked and uncracked sections respectively; I_m, I_{e1} and I_{e2} are the effective moments of inertia at the mid-span and at both ends respectively; and I_{exp} is the experimental value of I_e. In

addition, M_{cr} and M_a are the cracking moment and the applied service moment respectively. The values of the exponent m in Eq.(3.1) is given by:

$$m = \frac{\log\left[\dfrac{I_{exp} - I_{cr}}{I_g - I_{cr}}\right]}{\log\left[\dfrac{M_{cr}}{M_a}\right]} \qquad (3.3)$$

The suggested value of m in Eq.(3.1) due to Branson (1965) is 3. For a load level greater than $1.5M_{cr}$, the reduction in the value of m is very small. Therefore, an accurate prediction of I_e can be computed from Eq.(3.1) with $m = 3$ provide that the loading level is greater than $1.5M_{cr}$. If the loading level is less than $1.5M_{cr}$, the value of $m = 3$ can still be used but the estimated value of I_e should be reduced by 10% (Al-Zaid et al., 1991). In this study, the range of loading level (M_a/M_{cr}) to determine the value of m varies from 1.5 to 4.0. Note that the value of I_e also depends on the reinforcement ratio, especially for heavily reinforced concrete members, and the cracked length of the member. Those effects are not considered in this study. In addition, the models mentioned above are valid when the section property is uniform along the span length, which is not the case under consideration in this paper.

In the case of a beam with fix-ended supports subjected to a central point load, the effective moment of inertia is calculated from the following equation

$$EI_{exp} = \frac{PL^3}{192\Delta} \qquad (3.4)$$

where P and Δ denote the magnitude of applied loading and the mid-span deflection respectively. For a given load-deflection diagram, the effective moment of inertia from either a finite element or an experiment result can be calculated by using Eq.(3.4). The effective moment of inertia can also be obtained from Eqs.(3.1) and (3.2) according to Branson (1965) for given values of weight factors and the exponent m. The appropriate values of weight factors and exponent m from both FEM and experiment results are determined by using the least square method with the initial values of (0.30,0.70) and 3 respectively for weight factors and m. It is found that the difference between the effective moment of inertia computed from Eqs.(3.1) and (3.2), and that from Eq.(3.4) is within 10 percent. According to Eq. (3.2), the weight factors are 0.3 and 0.7 for negative and positive bending moments respectively. The weight factors computed from finite element analysis are (0.22, 0.78) and (0.31, 0.69) for

LS_F and LS_S slabs respectively. The weight factor for the negative bending moment of the LS_F slab is less than that of the LS_S slab since the length of lap reinforcement at the mid-span of the LS_F slab is much longer. As a result, the mid-span section of the LS_F slab is stiffer and the negative bending moment zone is then shorter. Note that the LS_H slab behavior does not follow the Branson based formula since this slab behaves like a cantilever slab.

The value of the exponent m in Eq. (3.1) was originally proposed to be 3 by Branson (1965). Al-Zaid, et al. (1991) later suggested that this value should be 2.8, 2.3 and 1.8 for a beam under uniformly distributed loading, third-point loading and mid-span concentrated loading respectively. Since the mid-span loading in this study is applied through a loading plate, which is not an actual point load, the proposed value for m varies from 1.8 to 2.3. It is found that the optimal values of m from the finite element analysis are 2.3 and 2.5 the for LS_F and the LS_S slabs respectively. This implies that the suggested value of m between 1.8 and 3 (Branson, 1965 and Al-Zaid et al., 1991) can not be used for the LS_H slab, which has no lap reinforcement and a large crack is concentrated at the mid-span section that behaves like a cantilever slab.

Three different thickness-to-span ratios, i.e. d/L = 200/2000, 300/2000 and 300/1000, which are widely employed in practical constructions, are considered for the LS_F, LS_S and LS_H slabs under end rotation and end translation. Only the finite element method is employed to determine the effective moment of inertia (I_e) since it is difficult to set up and control these two types of boundary conditions in the full-scale testing. In the case of end rotation, the exponent m for the effective moment of inertia is calculated from the following equation

$$EI_{exp} = \frac{M_a L}{2\theta}$$ (3.5)

where θ is the end rotation angle and M_a in Eq.(3.5) is the moment due to reduced stiffness and end rotation, which is different from the mid-span loading case where M_a is computed from the applied load and it does not depend on stiffness. It is found that the estimated values of m are equal to 0.5, 0.8 and 0.3-0.5 (depending on the thickness-to-span ratio of the link slab) for the LS_F, LS_S and LS_H slabs respectively as shown in Fig. 3.14(a) and the difference between the effective moment of inertia computed from Eq.(3.5) and that from Eq.(3.1) is less than 10 percent. Caner (1996) has also proposed the effective stiffness of link slabs in his program,

however, the effect of lap reinforcement is not included in his model. It has been shown that the value of $m = 0.8$ from this study of LS_S is close to $m = 1$ from his study because of the similar behavior of this detailing and a link slab without lap reinforcement.

Finally, the exponent m for the translational loading case is given by

$$EI_{exp} = \frac{M_a L^2}{6\Delta} \tag{3.6}$$

where Δ is the support settlement and M_a is the moment due to reduced stiffness and end translation. The estimated value of m in this case ranges from 0.70 to 0.90 for all lengths of lap reinforcement (see Fig. 3.14(b)) and the difference between the effective moment of inertia computed from Eq.(3.6) and that from Eq.(3.1) is less than 10 percent. This is due to the fact that the maximum bending moment for translational loading is close to the ends of the slabs, where the section properties are identical for all types of reinforcement detailing. In addition, the bending moment at the mid-span, in which the section properties for each link slab are different, is zero.

3.3 Interaction Model

A multi-span elevated highway with a number of precast prestressed concrete girders with simple supports over the piers undergoes an increased deformation over time due to creep under a sustained prestressing force and other effects. No restraint moments are induced at the ends of simply supported girder. However, when the girder ends are restrained by link slab and support as in the case of jointless bridges, then the bridge becomes a statically indeterminate structural system, allowing secondary forces to develop due to creep, shrinkage, steel relaxation and temperature effects. A good understanding of the behavior of jointless bridges with link slabs under the restraint is essential in order to appropriately design the continuity link slab connection.

The girder end movements and the behavior of link slabs are shown in the previous section. The boundaries of link slabs can be categorized into axial deformation, end rotation and end translation while the force in link slabs can be determined by a product of link slab stiffness for each nodal degree of freedom and their end movements (Fig. 3.15). However, these end movements are restrained by the

stiffness of adjacent girders and supports which are considered in this chapter. The end restraints can be separated into two parts which are axial deformation – end rotation restraint and end translation – mid-span loading restraint. The theoretical model to study this problem must be modeled by the boundary condition as shown in Fig. 3.16 (a) and (b).

3.3.1   *Axial Deformation – End Rotation Restraint*

Continuous structural systems can be analyzed using several conventional methods such as moment distribution, the conjugate beam method and three-moment equations. However, the unconventional nature of the behavior of continuous bridge girder systems, where continuity is due to joining concrete decks only, makes it necessary to use a refined analysis such as the finite element method (FEM). Analyzing any of these configurations requires the use of advanced tools such as FEM to be able to correctly account for the specifics of the behavior. Plane elements with two translation degrees of freedom at each node were used to model girders and link slabs.

The link slab that connects decks on both sides of an inner support makes the behavior of the partially continuous system complicated as compared to fully continuous systems. The difference between the behavior of the partially continuous system and that of a simply supported system is that the girders are prevented from rotating freely because of the existence of the link slab. Deformations in the girders lead to the deformation of the link slab. As a result, a force develops in the link slab, which generates a continuity moment at this inner support.

The support conditions of elastomeric bearings as normally used for precast girders and these arrangements are shown in Fig. 3.17: the higher horizontal stiffness of elastomeric bearings is applicable to a structure at the central portion of continuous multiple spans where there is restraint from longitudinal movement and the lower horizontal stiffness of elastomeric bearings is applied at the end portion of continuous multiple spans where restraints are allowed freer longitudinal and rotational movement. The type of support affects the behavior of the system and the difference in reactions leads to different behaviors. Dealing with each of the two support conditions is different. For simplicity, the hinged support configuration will be referred to as RHHR and roller support configuration as RRRR, where H stands for a

hinged support and R a roller support. The theoretical model to study this problem must be modelled by the boundary condition as shown in Fig. 3.17 (a) and (b).

The variables that are considered in this study are the degrees of stiffnesses of both girders and link slabs which are dependant on section properties and span length. For the girder part, the distance from the bottom face to the centroid of girder section (*Cb*) and the ratio of moment of inertia to sectional area (*I/A*) are controlled to be reasonable constants in order to neglect other effects that are not included in this study. In addition, the range of chosen relative stiffness of composite girders and link slabs ($[EI/L]_{\text{composite girder}}/[EI/L]_{\text{link slab}}$) is realistic for existing typical girders as shown in Fig. 3.18 dependant on dimensions and cracking in link slabs. The restraints due to elongation and rotation of girders are analyzed by the finite element method to clarify the restraint behavior in term of the center of rotation. Restraints of end movements of both longitudinal and rotational ones are affected by the stiffness of the link slab, stiffness of girders, support conditions or horizontal stiffness of bearing pads, besides the height (*H*), support level (*x/H*) and the centroid of girders (*Cb/H*) which are varied in this study as shown in Table 3.8.

The internal forces of link slabs can be determined by the matrix using stiffness matrix of link slab associated with restrained end movements of elongation, rotation and translation as inputs. Consequently, if there are some fixed end forces due to loading on link slabs acting on the structure, then the equation can be written as:

$$[P]=[K][u]+[P]_{FEM} \tag{3.7}$$

where [*P*] is nodal force or internal force of link slab

[*K*] is the effective stiffness of link slab.

[*u*] is nodal movement due to restraint of end movements.

$[P]_{FEM}$ is fixed end force due to loading on link slab.

The end movements considered in this study are shortening, elongation axial deformation and downward, upward end rotation. In this part, each type of end movement of simply supported highway girders will be independently restrained by link slabs in terms of unit deformation to consider their behaviors and their results on the variations.

3.3.1.1 Axial Deformation

The axial deformation of highway girders occurs from axial deformation of each structure, both main girders and link slabs, due to ambient temperatures, creep, and shrinkage. However, the axial deformation of link slabs can be neglected because slab length is much less than girder length. Axial deformation of main girders causes both axial and end rotational movements of link slab boundary conditions in the multi-span girders. Restraints are related to the stiffness of both girders and link slabs as well as the support configuration and height of the girders.

The influence of relative stiffness of the girder and the link slab ($[EI/L]_{composite\ girder}/[EI/L]_{link\ slab}$), support configuration (R-R, and H-H), height of girders (H), support level (x/H) and distance from the bottom face to the centroid (Cb/H) of girders is shown in Fig.3.19(a)-(d) in the form of axial and rotational restraint of link slab per 1 unit axial deformation of girders.

Rotational and axial restraints in link slabs due to axial deformation in girders are less affected by the support level (x/H) in R-R support condition and are less affected by the centroid of girders (Cb/H) in H-H support condition.

If the supports are elastomeric bearing pads, the axial restraint is quite low and this seems to be the behavior that occurs with the R-R support configuration because the horizontal stiffness of elastomeric bearing pads is much smaller than other axial stiffness. For more accurate amounts of axial restraints in link slabs in the multi-span girders, the whole superstructure seems to float on elastomeric bearing pads and the force occurred by elastomeric bearing deformation which is transferred through link slab and is dependant on movement in each position which can be determined except the breaking force from truck load. This force causes girder and link slab deformation which is one of the nodal movement matrix in Eq. (3.7). (Fig. 3.20)

$$[P] = [K][\Delta_H] \tag{3.8}$$

where $[P]$ is nodal force due to elastomeric bearing deformation depended on movement at each position

$[K]$ is longitudinal stiffness

$[\Delta_H]$ is horizontal movement which is one of the nodal movement matrices in Eq. (3.7).

The axial force in link slabs results from the axial deformation of link slabs which is equal to the different horizontal movement between both ends.

The results from the longitudinal interaction model conclude that the axial force in link slabs depends on the horizontal stiffness of elastomeric bearings, longitudinal movement and link slab position. Maximum longitudinal movement is at the free end of the whole superstructure and minimum stiffness of bearing pads is usually used at this position. So the maximum axial force in link slabs is at the mid-length of the whole superstructure because it results from a summation of elastomeric bearing pad forces from that position to edge position. Compared to rotational and translation restraints, axial restraint is not dominated and can be controlled.

3.3.1.2 End Rotation

Because the link slab is assumed to be linear and flexible in comparison with end stiffness of the girders and the girders are directly connected to link slabs, the end movement of girders and link slabs is considered to be similar. Although the stiffness of link slabs is much less than the stiffness of girders and sometimes the girders are assumed to be simply supported, the girders are still restrained by adjacent link slabs and supports. End rotation of the main girder causes both axial and rotational restraints in link slabs of the multi-span girders. From the deflected end rotation of girders, the center of rotation at the section of girder-link slab connection is located at different positions depending on support configuration as shown in Fig. 3.21. The influence of relative stiffness ($[EI/L]_{\text{composite girder}}/[EI/L]_{\text{link slab}}$), support configuration (R-R and H-H), height of girder (H), support level (x/H) and distance from the bottom face to the centroid (Cb/H) of girder is shown in Fig. 3.22(a)-(d) in the form of axial and rotational restraints of link slab per 1 unit end rotation of deflected girder.

For the R-R support condition, the support level (x/H) does not significantly affect both axial and rotational restraints. A rise in the relative stiffness increases the rotational restraint to be 1.00 times that of simply supported end rotation. When the relative stiffness is more than 10, the reduction of rotational restraint is less than 5% of the simply supported end rotation and it is less affected by Cb/H and height of girders (H). Whereas, the relative stiffness is less than 10, the more height and Cb/H of girders it is, the more rotational restraint there is. The axial restraint of link slabs can be neglected because the whole superstructure seems to float on roller, so it results from elongation of main girders only as previously mentioned. Nevertheless, the more height (H) and less Cb/H of girder there is, the more axial restraint there is.

A decrease in relative stiffness reduces the axial and rotational restraints in link slabs for the H-H support condition. A fall in axial and rotational restraints result from a rise in the height of girders (H) and a fall in support levels (x/H). When the girder is deflected, the axial restraint of link slabs is tension and increases with an increase in end rotation because the center of rotation is at the hinged support. However, Cb does not significantly affect the axial and rotational restraints of link slabs for the H-H support condition.

In the case of elastomeric bearing pad installation, the R-R support configuration can represent its behavior because the elastomeric bearing pad is stiff and strong with respect to vertical loads and flexible with respect to shear compression and rotation. The direct stiffness method is used to determine the rotational restraint with only the flexural stiffness of both girder and link slab.

$$[P] = [K][\theta] \tag{3.9}$$

where $[P]$ is the nodal force due to end rotation and stiffness of girder

$[K]$ is the rotational stiffness of the system

$[\theta]$ is the rotation of the link slab which is one of the nodal movement matrix in Eq. (3.7).

3.3.2   End Translation – Mid-span Loading Restraint

If supports are considered as an elastomeric bearing pad, a differential support settlement can occurr. Because the flexural stiffness of girders is much more than the flexural stiffness of link slabs, the behavior of link slabs is fixed-end slab by adjacent girders in translation analysis. However, the girders are supported by elastomeric bearing pads and their supports are settled when moving load passes. Translational restraints are subjected to flexural stiffness of link slabs and the vertical stiffness of elastomeric bearing pads.

The real structure would be replaced by the structural model (Fig. 3.23(a)). The direct stiffness method should be used to determine the stress in link slabs. The fixed-coordinate solution and joint release solution model are shown in Fig. 3.23(b) and (c). The notation of these models is shown below.

P is the moving point load or truck load

$w(x)$ is the distributed load or dead load

L is the span length of link slabs

k_A, k_B is the vertical stiffness of elastomeric bearing pads

E, I is the elastic modulus and moment of inertia of link slabs

From Fig. 3.23(a), (b) and (c) the principal of superposition can be used to give the structural global stiffness as follows.

$$[K] = \begin{bmatrix} 12EI/L^3 + k_A & -12EI/L^3 \\ -12EI/L^3 & 12EI/L^3 + k_B \end{bmatrix} = \frac{12EI}{L^3} \begin{bmatrix} 1 + \alpha_A & -1 \\ -1 & 1 + \alpha_B \end{bmatrix} \tag{3.10}$$

where $\alpha_{A,B} = \dfrac{k_{A,B} L^3}{12EI}$ is the vertical relative stiffness (elastomeric bearing vertical stiffness – to –link slab flexural stiffness ratio)

The moving point load on the spring support makes it possible to calculate the maximum differential support settlement from the axle load of the adjacent span with longitudinal and transverse distribution factors. The ratio of the translational restraint to free vertical settlement is related to the vertical relative stiffness ($Kv/[12EI/L^3]_{\text{link slab}}$) as shown in Fig. 3.24. The more flexural stiffness of link slabs reduces the differential settlement because the point load can be better distributed to adjacent elastomeric bearing supports and vice versa. The differential settlement is used to determine internal forces which are both flexure and shear forces.

In this part the shear force, moment at support and mid-span of link slab are determined. Flexural moments at each support are:

$$\begin{bmatrix} M_A \\ M_B \end{bmatrix} = \frac{wL^2}{12} \begin{bmatrix} 1 \\ -1 \end{bmatrix} + \frac{Px(L-x)}{L^2} \begin{bmatrix} L-x \\ -x \end{bmatrix} + \frac{PL[(\alpha_A + \alpha_B)x - \alpha_B L]}{2(\alpha_A \alpha_B + \alpha_A + \alpha_B)} \begin{bmatrix} 1 \\ 1 \end{bmatrix} \tag{3.11}$$

And moment at mid-span is:

$$M_{CL} = \frac{Px}{2} - \frac{Px(L-x)}{2L} + \frac{wL^2}{24} ; 0 < \text{x} \le \text{L/2} \tag{3.12a}$$

$$M_{CL} = \frac{P(L-x)}{2} - \frac{Px(L-x)}{2L} + \frac{wL^2}{24} ; \text{L/2} < \text{x} \le \text{L} \tag{3.12b}$$

In addition, shear forces at each support are:

$$\begin{bmatrix} V_A \\ V_B \end{bmatrix} = \frac{wL}{2} \begin{bmatrix} 1 \\ 1 \end{bmatrix} + \frac{Px(L-x)(L-2x)}{L^3} \begin{bmatrix} 1 \\ 1 \end{bmatrix} + \frac{P}{L} \begin{bmatrix} L-x \\ x \end{bmatrix} + \frac{P[(\alpha_A + \alpha_B)x - \alpha_B L]}{(\alpha_A \alpha_B + \alpha_A + \alpha_B)} \begin{bmatrix} 1 \\ -1 \end{bmatrix} \tag{3.13}$$

And shear force at mid-span is:

$$V_{CL} = \frac{Px(L-x)(L-2x)}{L^3} + \frac{P(L-x)}{L} - P ; 0 < \text{x} \le \text{L/2} \tag{3.14a}$$

$$\frac{Px(L-x)(L-2x)}{L^3}+\frac{P(L-x)}{L}; L/2 < x \leq L \qquad (3.14b)$$

The vertical relative stiffness (α_A, α_B) and link slab span length are set to be the parameters in this study. The terms of w(x) in Eq. (3.11) – (3.13) can be neglected because it is a constant term so only the terms dependant on moving loads are considered and it can be concluded as follows. .

1. An increase in vertical relative stiffness (α) makes the supports of link slabs unsettled. When vertical relative stiffness (α) increases to an infinite value and the point load moves on both supports, the moment at support (M_A) falls to zero. The maximum negative moment at support (M_A^-) happens when the point load moves by around 0.2L to 0.4L. The maximum shear force at support ($V_{A,max}$) happens when the point load moves around supports and is equal to that point load.

2. A decrease in vertical relative stiffness (α) makes the supports of link slabs settled. The maximum different settlement of supports occurs when the point load moves close to the support and maximum moment at support ($M_{A,max}$) rises to $PL^2/4$ (the third term in Eq. (3.11)). The moment at support (M_A) will be zero or will change to another direction when the point load moves by around 0.25L. The maximum shear force ($V_{A,max}$) happens when the point load moves by around 0.2L for a shorter span (L=1m.). In addition, the maximum shear force ($V_{A,max}$) is equal to the point load and happens when the point load moves around L for a longer span (L=2 m.).

3. If vertical relative stiffness at support A (α_A) is much more than vertical relative stiffness at support B (α_B), the maximum different settlement of supports occurs and the maximum moment at support A ($M_{A,max}$) rises to $PL^2/2$ when the point load moves around x=L. When the point load moves around x=0, the minimum different settlement and minimum moment at support A ($M_{A,min}$) occurs and equals around zero and vice versa. In addition, the shear force at support (V_A) that point load is around x=0 is approximately point load, P (the third term in Eq. (3.13)). When the point load is around x=L, the shear force at support (V_A) is approximately PL (the fourth term in Eq. (3.13)).

4. The value of maximum shear at support ($V_{A,max}$), maximum moment at support ($M_{A,max}$), and the position of the point load that produces them are dependant on span length also. An increase in span length and more different vertical relative stiffness increases the additional shear and moment.

The moment and shear at support are varied by vertical relative stiffness, point load position and span length. It can be found that the boundary of vertical relative stiffness is dependant on point load position and span length. Because mid-span moment is equal to $PL/8$ independed of the vertical relative stiffness, the boundary of vertical relative stiffness for limited moment at support ($PL/8$) can be derived from Eq. (3.11) when the vertical relative stiffness is in the boundary of:

$$\alpha \geq 4L - 2 \, ; \, M_{x=L} = PL/8 \tag{3.15a}$$

$$\alpha \leq 5.263L - 2 \, ; \, M_{x=0.4L} = PL/8 \tag{3.15b}$$

as shown in Fig. 3.25. Moreover, the boundary of vertical relative stiffness for limited shear at support that is limited by P also can be derived when the vertical relative stiffness is in the boundary of:

$$\alpha \geq L - 2 \, ; \, V_{x=L} = P \tag{3.15c}$$

as also shown in Fig. 3.25.

If the shear and flexural strength along span length is similar, external factored shear and moment at support and mid-span will be considered as a designed section along span length following the above boundary. If the vertical relative stiffness (α) on both supports has to be different, moment and shear in this case will be more than them in the same vertical relative stiffness case.

3.3.3 *Interaction of Restraints*

Longitudinal and rotational movements of simply supported girders are used to determine axial deformation – end rotation restraint of link slabs by superposition of their restraints following Figs. 3.19 and 3.22. Domination of axial or rotational restraint in link slabs is dependant on their restraints and free end movement of highway girders. The axial and rotational restraints of link slabs are divided by link slab length to convert to axial strain and curvature along the link slab. In addition, the end translation – mid-span loading restraint also affects the additional restraint in the

link slab. From the known restraints of link slabs which are axial deformation, end rotation and end translation, the internal forces of link slabs can be calculated by Eq. (3.7).

In the previous part, only a 2-span jointless elevated highway with link slabs was considered with the variations. In the case of elastomeric bearing being used supports of a 6-span jointless elevated highway, the interaction behavior is close to the R-R support condition as shown in Fig. 3.26.

The 6-span jointless bridge with link slabs and roller supports is studied to considered the amount of restraint in link slabs and the comparison between end restraints at each position of end girders from section 3.3.1 – 3.3.2. Figures. 3.27 - 3.28 show the end restraints at each position of multiple spans highway girder from 1 unit axial deformation and end rotation of highway girders. The sign convention of axial and rotational restraints is positive when the link slab is compressed and upwardly bent respectively.

The rotational restraint of link slabs per 1 unit elongation of girders at each position at 1st to 5th position have the same trend as the R-R case but end rotation at the 6th position is smaller and tends to be zero when the relative stiffness is more than 10.

The axial restraint of link slabs per 1 unit elongation of unrestrained girder at each position also follow the same trend as the R-R case with some increases depending on the position in different directions.

The rotational restraint of link slabs per 1 unit end rotation of girder at 1st to 5th positions are close to R-R case with some reduction, however, the end rotation at 6th position is more than the R-R case which must be taken into consideration for expansion joint design. The axial restraint of link slabs per $(x10^{-3}$ rad) unit end rotation of unrestrained girder at each positions is quite similar.

The four maximum cases of end movements as shown in Fig. 3.5 and Tables 3.5 – 3.6 and the relative degrees of stiffness ranging from 1 to 100 are used to determine the restraints in link slabs. Using 2 maximum cases of end movements and the above end restraints, the axial restraint due to the maximum shortening cases and the rotational restraint due to the maximum deflected case are shown in Figs. 3.29 and 3.30 with the variations in span length and relative stiffness. From the axial restraint, the more effective stiffness there is, the more axial restraint there is. However, the maximum axial restraint is still less than the cracking restraint in link slabs. So the

axial restraint does not dominate compared with the rotational restraint. When the relative stiffness is more than 10, the rotational restraint due to the maximum deflected case at each position of the link slab is quite similar. The horizontal stiffness of elastomeric bearings affects the additional axial restraint in link slabs that should be taken into consideration in the design of link slabs especially at 1st position (mid-length of the multiple span).

The flexure and shear forces from end translation due to elastomeric bearing settlement and mid-span loading should also be considered in the design especially at 4th and 5th positions where the vertical stiffness is less than other positions. However, both flexure and shear force can be controlled by the limitation of vertical relative stiffness ($Kv/[12EI/L^3]_{link\ slab}$).

From the possible range and severe case of elastomeric bearing stiffness, the horizontal stiffness of elastomeric bearing is quite low and the vertical stiffness is quite high as shown in Fig. 3.31, so the axial restraint from bearing and flexure restraint from the bearing settlement does not dominate compared with axial and flexure restraints from end movements. The flexural strain from wheel load on mid-span link slabs is also not dominant.

These restraints affect link slab stiffness and the relative stiffness as well. So the link slab stiffness mentioned above should be effective stiffness under restraints. The Branson-based model of effective stiffness can be used for approximate stiffness. The flexural restraint due to end rotation is the significant mode for the interaction model of multi-span jointless elevated highway with link slabs and elastomeric bearings. So the interaction chart of the effective moment of inertia, end rotation, and moment can be done as shown in Fig. 3.32 to be a tool for preliminary design. From this chart it can be seen that moment due to end translation and mid-span loading is quite less than moment due to end rotational restraint.

All components of restraint produce internal forces including moment, shear, and axial force in link slabs. Firstly, axial restraint should be designed in order to control allowable stress and crack width to ensure that cracks can be perfectly closed after unloading. Next, moment and shear restraints as follows:

$$M = \frac{PL}{8} + \frac{3EI}{L} \cdot \theta \qquad (3.16)$$

$$V = P + \frac{12EI}{L^3} \cdot \Delta \qquad (3.17)$$

should be designed for reinforcement by the code or the strut-and-tie method for reinforcement in link slabs with consideration of final performance including strength, serviceability and durability.

Table 3.1 Sectional properties of typical girders

Properties	I	T	U(1.50)	U(1.75)	Box (D2)	Box (D3)
Height (H, m)	1.70	1.77	1.50	1.75	2.40	2.40
Span Length (L, m)	21-30	30	22-27	25-32	25-45	30-48
Spacing (m)	2.67	2.57	3.375	3.375	10.2	13.7
Sectional Area (A, m^2)						
Precast	0.570	0.695	0.817	0.885	4.945	6.400
Composite	1.104	1.209	1.492	1.560	-	-
Moment Inertia (I, m^4)						
Precast	0.1967	0.2679	0.1861	0.2777	3.5941	4.8600
Composite	0.4522	0.4621	0.4863	0.6831	-	-
Volume to Surface ratio (V/S, mm)						
Precast	115	82	104	101	144	143
Composite	121	144	112	109	-	-
Distance from the bottom face to the centroid of girder section (Cb, m)						
Precast	0.8407	1.0628	0.7021	0.8238	1.6248	1.6451
Composite	1.3047	1.4060	1.1083	1.2679	-	-

Table 3.2 Description of girder model

	Precast member	Cast in-situ deck
Concrete strength (ksc)	400 ksc	300 ksc
Volume-to-surface ratio (mm)	120 mm	
Relative humidity (%)	80 %	
Construction sequence		
- Release of prestressing	3-day	
- Deck casting	60-day	
- Composite action after	62-day	3-day

Table 3.3 Axial deformation contributed from each source

Cross section	Span length (m)	Axial deformation (mm)				
		Long-term effects	Temperature Gradient before deck casting	Temperature Gradient at service time	Live Load	Ambient temperature
		[1]	[2]	[3]	[4]	[5]
I	22	-4.90823	0.672598	1.169572	0.994024	3.025
	26	-5.52265	0.794889	1.382221	1.51102	3.575
	30	-6.86517	0.339301	1.558671	2.051762	4.125
T	30	-5.80693	1.435641	1.585425	1.388909	4.125
U-1.5	22	-5.95291	0.491765	0.903741	0.848414	3.025
	26	-7.03526	0.581177	1.068058	1.289677	3.575
U-1.75	26	-6.88806	0.585572	1.013267	1.003671	3.575
	32	-8.47762	0.720703	1.247098	1.703473	4.4
Box-D2	23	-5.40399	1.421492	1.420359	-0.08197	3.1625
	34	-8.55906	2.116456	2.119648	-0.29162	4.675
	44	-12.2873	2.739874	2.743941	-0.71754	6.05
Box-D3	30	-6.39029	1.85321	1.82066	-0.23712	4.125
	37	-9.5768	2.409039	2.410437	-0.40907	5.0875
	47	-12.9705	3.059549	3.061056	-0.87735	6.4625

Table 3.4 Rotation contributed from each source

Cross section	Span length (m)	Rotation (rad)				
		Long-term effects [1]	Temperature Gradient before deck casting [2]	Temperature Gradient at service time [3]	Live Load [4]	Ambient temperature [5]
I	22	-9.03E-04	-1.29E-03	-9.32E-05	2.11E-03	-
	26	-5.86E-04	-1.52E-03	-1.10E-04	3.04E-03	-
	30	-6.93E-04	-2.79E-04	-1.69E-04	4.07E-03	-
T	30	2.06E-05	-2.15E-03	-2.39E-04	3.30E-03	-
U-1.5	22	-1.07E-03	-1.26E-03	-2.73E-04	2.14E-03	-
	26	-1.26E-03	-1.48E-03	-3.23E-04	3.10E-03	-
U-1.75	26	-1.35E-03	-1.25E-03	-5.37E-04	2.52E-03	-
	32	-1.66E-03	-1.53E-03	-6.61E-04	3.93E-03	-
Box-D2	23	-5.37E-05	-1.22E-03	-1.22E-03	1.33E-03	-
	34	-1.33E-03	-1.77E-03	-1.77E-03	2.66E-03	-
	44	-2.99E-03	-2.29E-03	-2.29E-03	4.38E-03	-
Box-D3	30	-9.79E-04	-1.52E-03	-1.51E-03	2.08E-03	-
	37	-2.17E-03	-1.90E-03	-1.90E-03	3.24E-03	-
	47	-3.61E-03	-2.42E-03	-2.41E-03	5.32E-03	-

Table 3.5 Maximum axial deformation cases

Cross section	Span length (m)	Maximum shortening combination of [1] – [2] – [5]		Maximum elongation combination of [4] + [3] + [5]	
		Axial deformation (mm)	End rotation (rad)	Axial deformation (mm)	End rotation (rad)
I	22	**-8.61**	3.87E-04	**5.19**	2.01E-03
	26	**-9.89**	9.38E-04	**6.47**	2.93E-03
	30	**-11.33**	-4.13E-04	**7.74**	3.90E-03
T	30	**-11.37**	2.17E-03	**7.10**	3.06E-03
U-1.5	22	**-9.47**	1.85E-04	**4.78**	1.87E-03
	26	**-11.19**	2.19E-04	**5.93**	2.77E-03
U-1.75	26	**-11.05**	-1.05E-04	**5.59**	1.99E-03
	32	**-13.60**	-1.29E-04	**7.35**	3.27E-03
Box-D2	23	**-9.99**	1.16E-03	**4.50**	1.07E-04
	34	**-15.35**	4.45E-04	**6.50**	8.94E-04
	44	**-21.08**	-7.01E-04	**8.08**	2.09E-03
Box-D3	30	**-12.37**	5.42E-04	**5.71**	5.68E-04
	37	**-17.07**	-2.72E-04	**7.09**	1.34E-03
	47	**-22.49**	-1.20E-03	**8.65**	2.91E-03

Table 3.6 Maximum end rotation cases

Section	Span length (m)	Maximum camber combination of [1] + [3]		Maximum deflection combination of [2] + [4]	
		Axial deformation (mm)	End rotation (rad)	Axial deformation (mm)	End rotation (rad)
I	22	-3.74	**-9.96E-04**	0.32	**3.40E-03**
	26	-4.14	**-6.96E-04**	0.72	**4.57E-03**
	30	-5.31	**-8.62E-04**	1.71	**4.35E-03**
T	30	-4.22	**-2.19E-04**	-0.05	**5.45E-03**
U-1.5	22	-5.05	**-1.34E-03**	0.36	**3.40E-03**
	26	-5.97	**-1.59E-03**	0.71	**4.58E-03**
U-1.75	26	-5.87	**-1.89E-03**	0.42	**3.77E-03**
	32	-7.23	**-2.32E-03**	0.98	**5.46E-03**
Box-D2	23	-3.98	**-1.27E-03**	-1.50	**2.54E-03**
	34	-6.44	**-3.09E-03**	-2.41	**4.43E-03**
	44	-9.54	**-5.28E-03**	-3.46	**6.67E-03**
Box-D3	30	-4.57	**-2.49E-03**	-2.09	**3.60E-03**
	37	-7.17	**-4.07E-03**	-2.82	**5.14E-03**
	47	-9.91	**-6.03E-03**	-3.94	**7.74E-03**

Table 3.7 Study program of link slab using MASA finite element analysis

Action	Details	Thickness-to-span ratio (mm/mm)		
		200/2000	300/2000	300/1000
Axial deformation	LS_H	LS_H_0.10	LS_H_0.15	LS_H_0.30
	LS_S	LS_S_0.10	LS_S_0.15	LS_S_0.30
	LS_F	LS_F_0.10	LS_F_0.15	LS_F_0.30
End rotation	LS_H	LS_H_0.10	LS_H_0.15	LS_H_0.30
	LS_S	LS_S_0.10	LS_S_0.15	LS_S_0.30
	LS_F	LS_F_0.10	LS_F_0.15	LS_F_0.30
End translation	LS_H	LS_H_0.10	LS_H_0.15	LS_H_0.30
	LS_S	LS_S_0.10	LS_S_0.15	LS_S_0.30
	LS_F	LS_F_0.10	LS_F_0.15	LS_F_0.30
Mid-span loading	LS_H	LS_H_0.10	LS_H_0.15	LS_H_0.30
	LS_S	LS_S_0.10	LS_S_0.15	LS_S_0.30
	LS_F	LS_F_0.10	LS_F_0.15	LS_F_0.30

Table 3.8 Study program of link slab using interaction model

Action	Support condition	Cb/H	Girder Height, H (m)	Support level, x/H		
				0	0.4	0.6
Axial Deformation / End Rotation	R-R	0.6	1.0	(0.6)(1.0)(0.0)	(0.6)(1.0)(0.4)	(0.6)(1.0)(0.6)
			1.5	(0.6)(1.5)(0.0)	(0.6)(1.5)(0.4)	(0.6)(1.5)(0.6)
			2.0	(0.6)(2.0)(0.0)	(0.6)(2.0)(0.4)	(0.6)(2.0)(0.6)
			2.5	(0.6)(2.5)(0.0)	(0.6)(2.5)(0.4)	(0.6)(2.5)(0.6)
		0.7	1.0	(0.7)(1.0)(0.0)	(0.7)(1.0)(0.4)	(0.7)(1.0)(0.6)
			1.5	(0.7)(1.5)(0.0)	(0.7)(1.5)(0.4)	(0.7)(1.5)(0.6)
			2.0	(0.7)(2.0)(0.0)	(0.7)(2.0)(0.4)	(0.7)(2.0)(0.6)
			2.5	(0.7)(2.5)(0.0)	(0.7)(2.5)(0.4)	(0.7)(2.5)(0.6)
	H-H	0.6	1.0	(0.6)(1.0)(0.0)	(0.6)(1.0)(0.4)	(0.6)(1.0)(0.6)
			1.5	(0.6)(1.5)(0.0)	(0.6)(1.5)(0.4)	(0.6)(1.5)(0.6)
			2.0	(0.6)(2.0)(0.0)	(0.6)(2.0)(0.4)	(0.6)(2.0)(0.6)
			2.5	(0.6)(2.5)(0.0)	(0.6)(2.5)(0.4)	(0.6)(2.5)(0.6)
		0.7	1.0	(0.7)(1.0)(0.0)	(0.7)(1.0)(0.4)	(0.7)(1.0)(0.6)
			1.5	(0.7)(1.5)(0.0)	(0.7)(1.5)(0.4)	(0.7)(1.5)(0.6)
			2.0	(0.7)(2.0)(0.0)	(0.7)(2.0)(0.4)	(0.7)(2.0)(0.6)
			2.5	(0.7)(2.5)(0.0)	(0.7)(2.5)(0.4)	(0.7)(2.5)(0.6)

(a) Creep coefficient

(b) Shrinkage strain

$$RE = 0.8\left[\frac{-log\left(t_{ps} - t_i\right) \times 24}{45} \times \left(\frac{F_{ps}}{A_{ps} \times 1.7 \times 10^8} - 0.55\right)\right] \times \frac{F_{ps}}{A_{ps}}$$
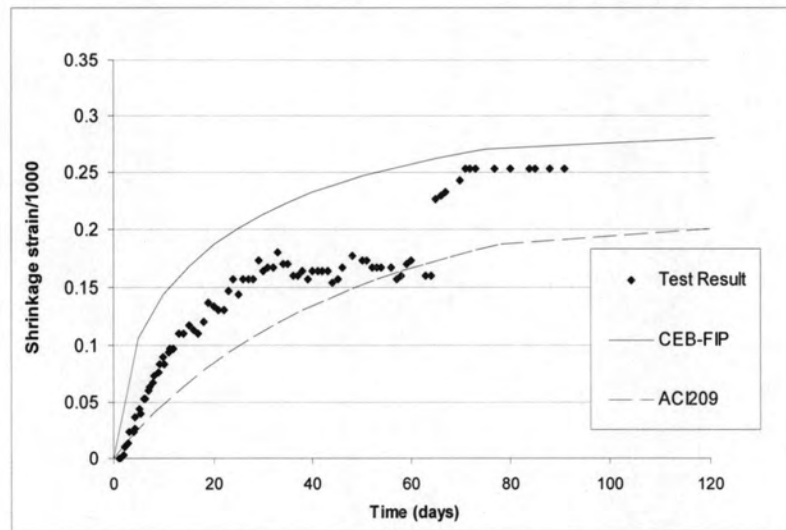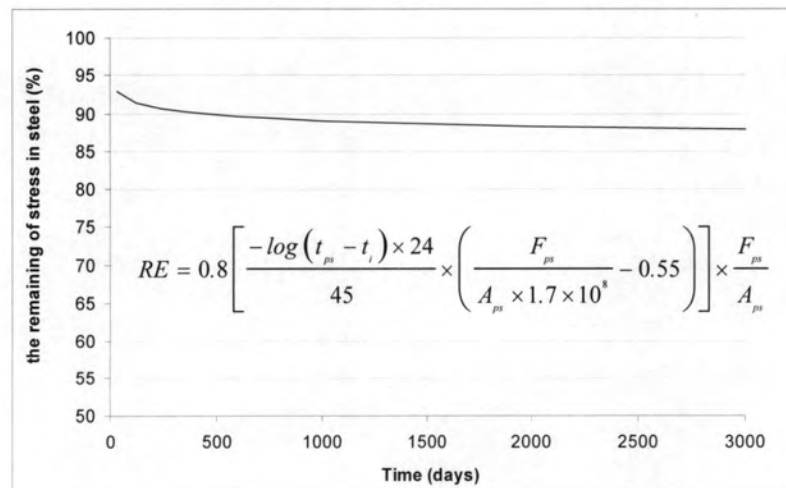
(c) Relaxation of prestressing steel

Fig. 3.1 Time-dependent effects
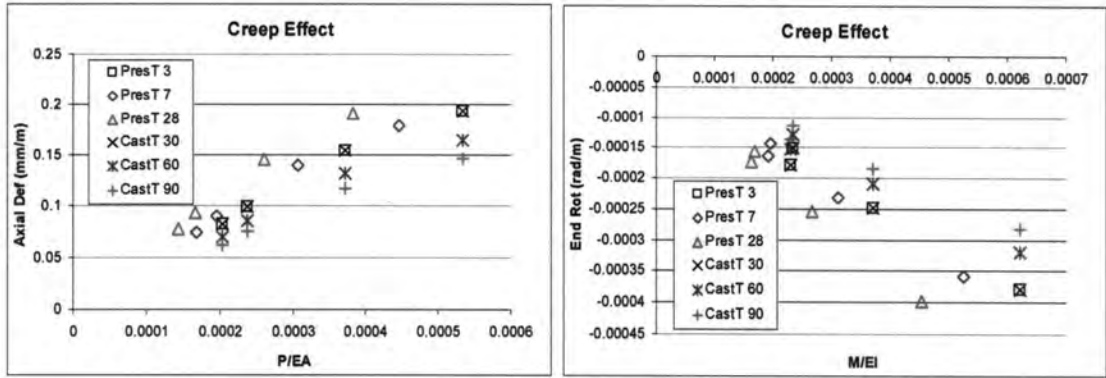
(a) Creep effect (CR)
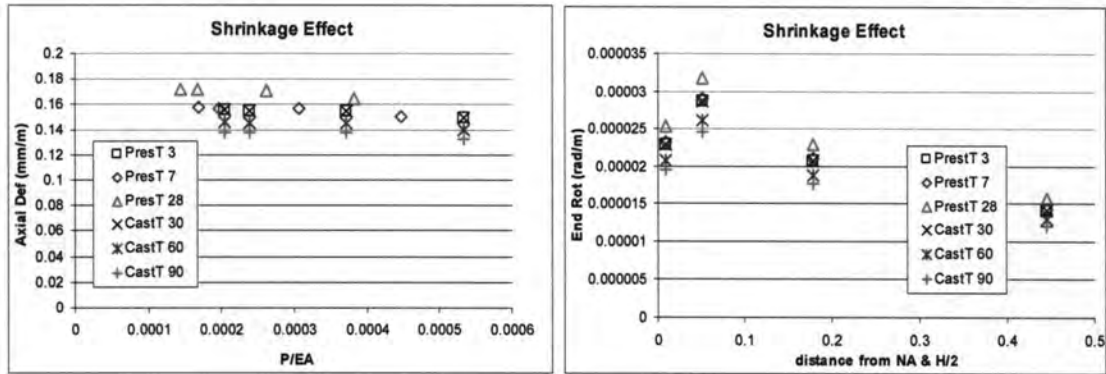
(b) Shrinkage effect (SH)
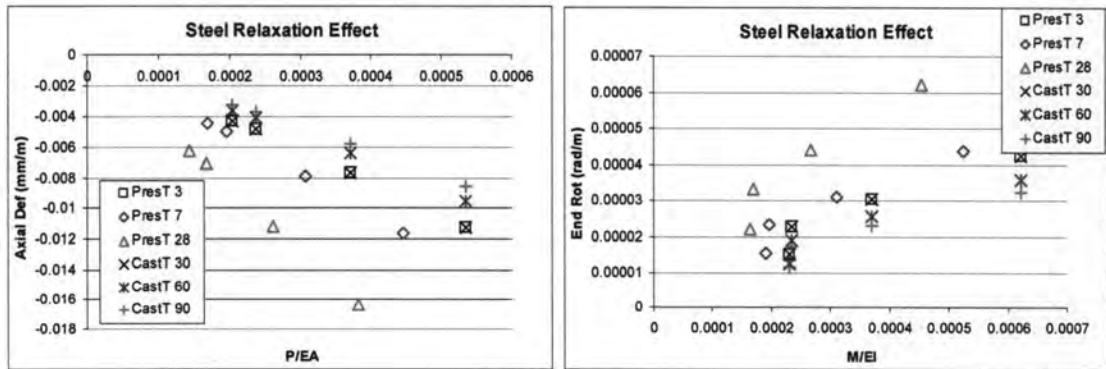
(c) Relaxation effect (RE)
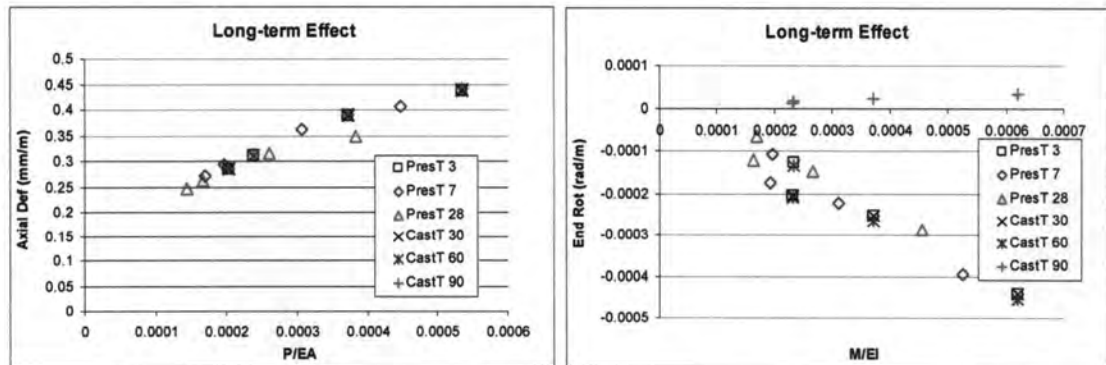
(d) CR+SH+RE effects

Fig. 3.2 End movements due to long-term effects of precast members
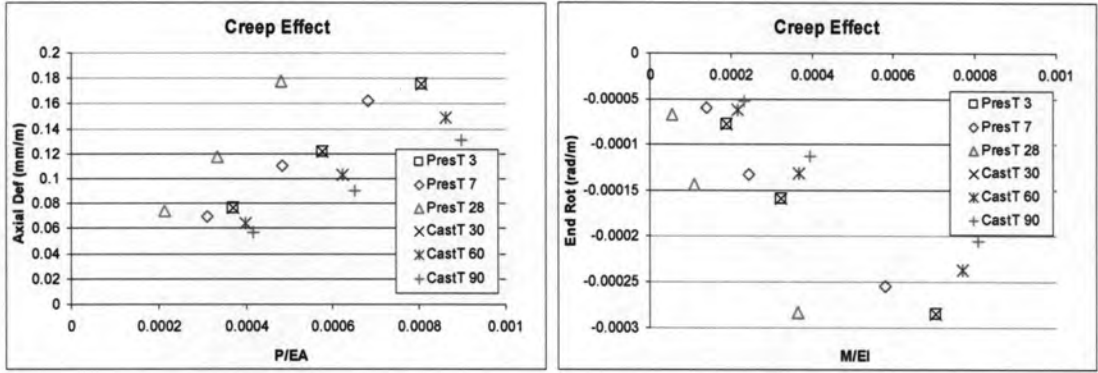
(a) Creep effect (CR)
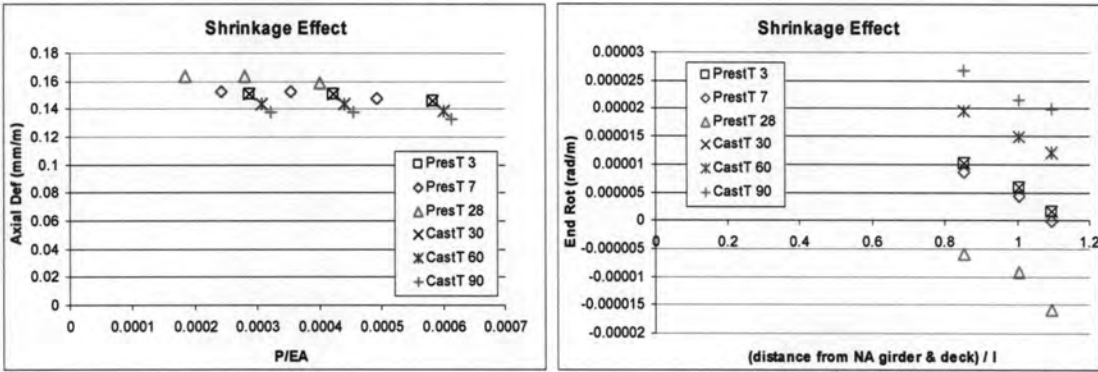
(b) Shrinkage effect (SH)
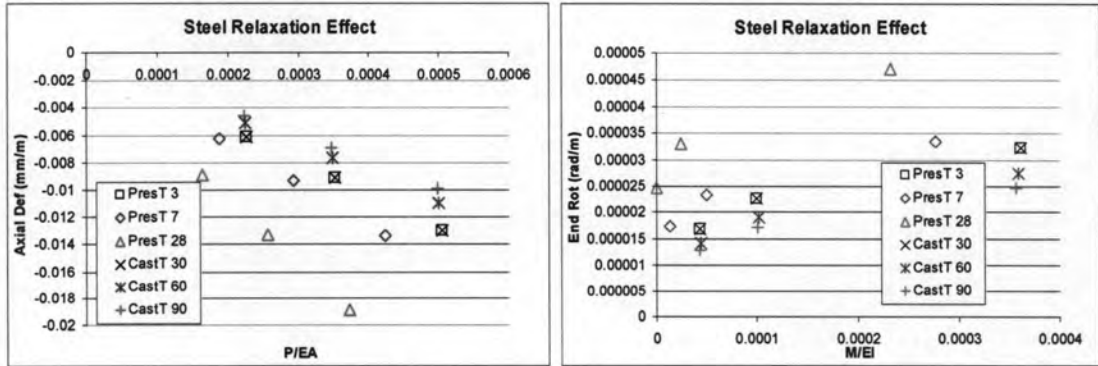
(c) Relaxation effect (RE)
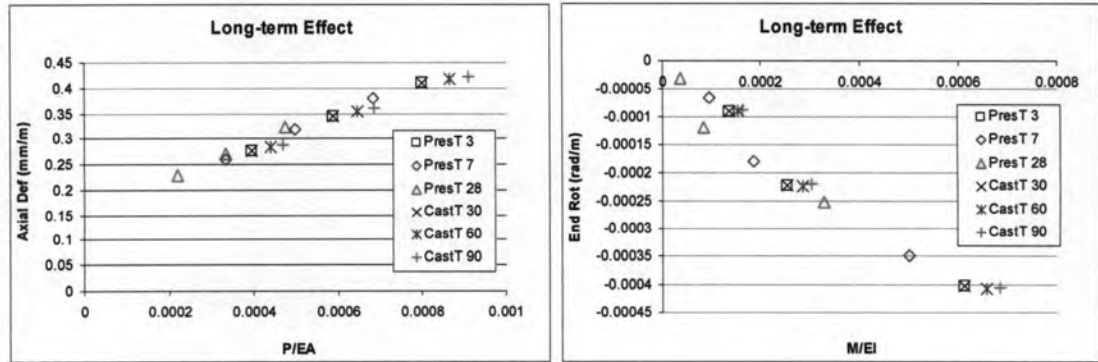
(d) CR+SH+RE effects

Fig. 3.3 End movements due to long-term effects of composite members
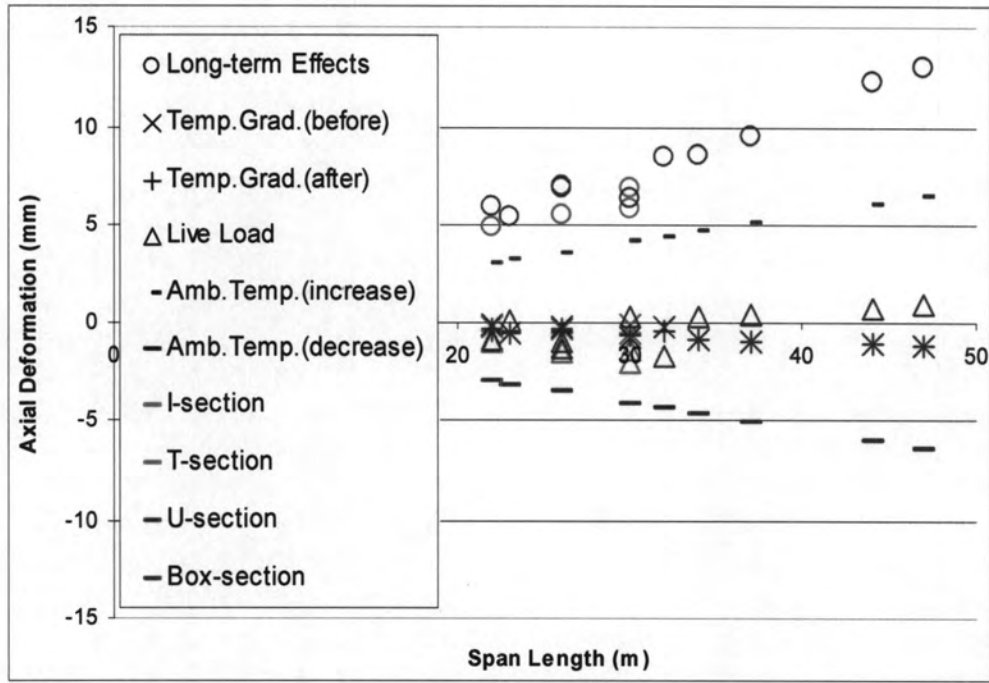
(a) Axial deformation

(b) End rotation

Fig. 3.4 End movements of typical girders

(a) Axial deformation

$y = -0.4374x$
$R^2 = 0.923$

(b) End rotation

$y = 0.0002x$
$R^2 = 0.7996$
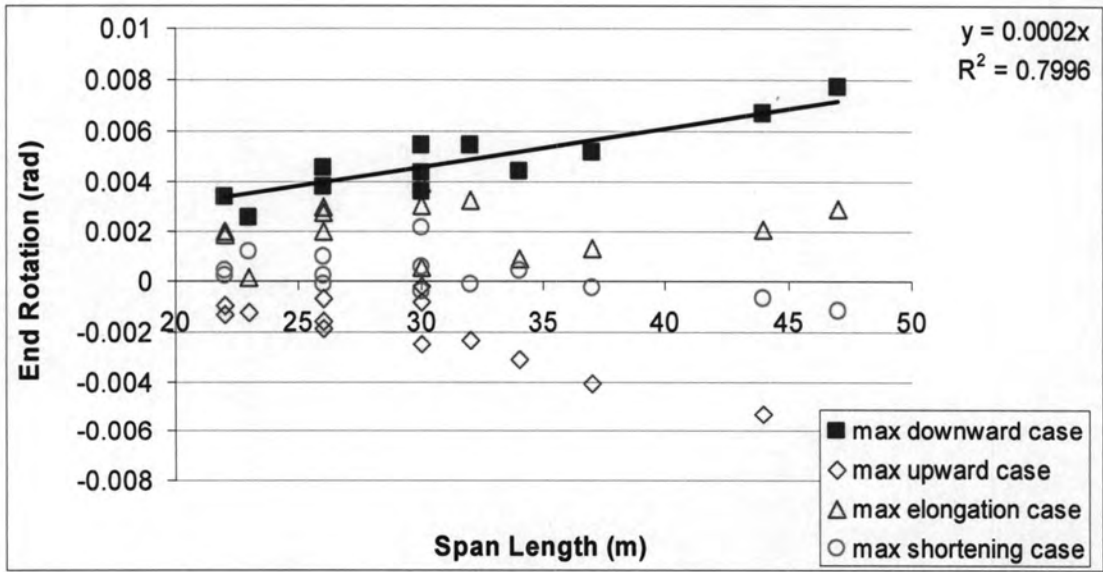
Fig. 3.5 Extreme cases of end movements
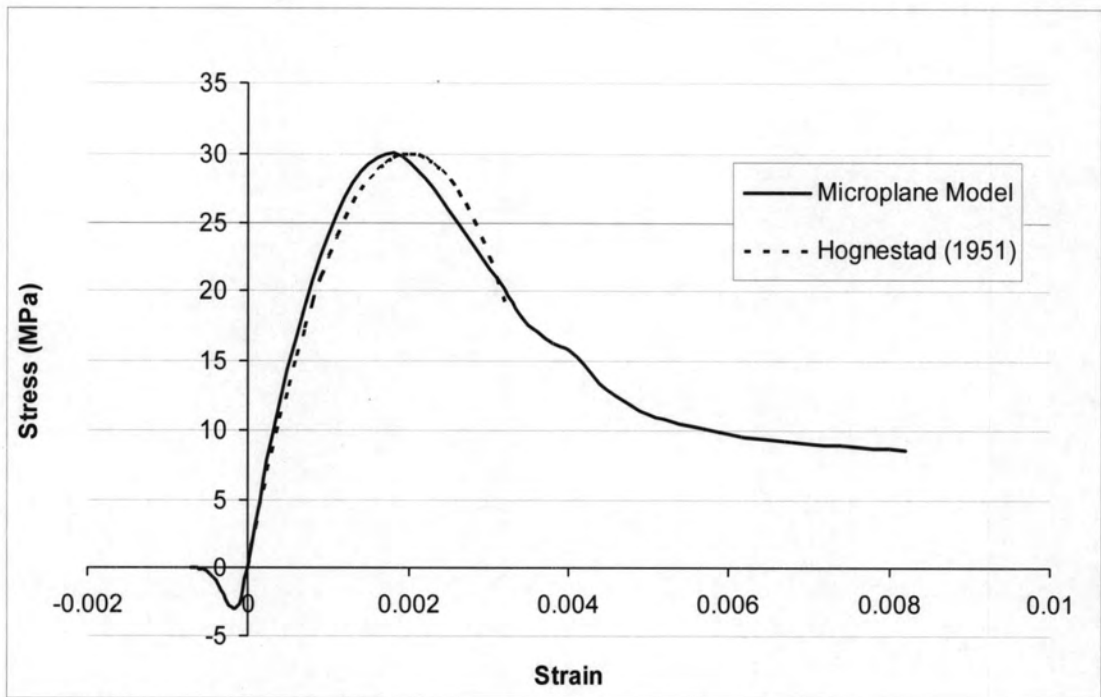
(a) Concrete
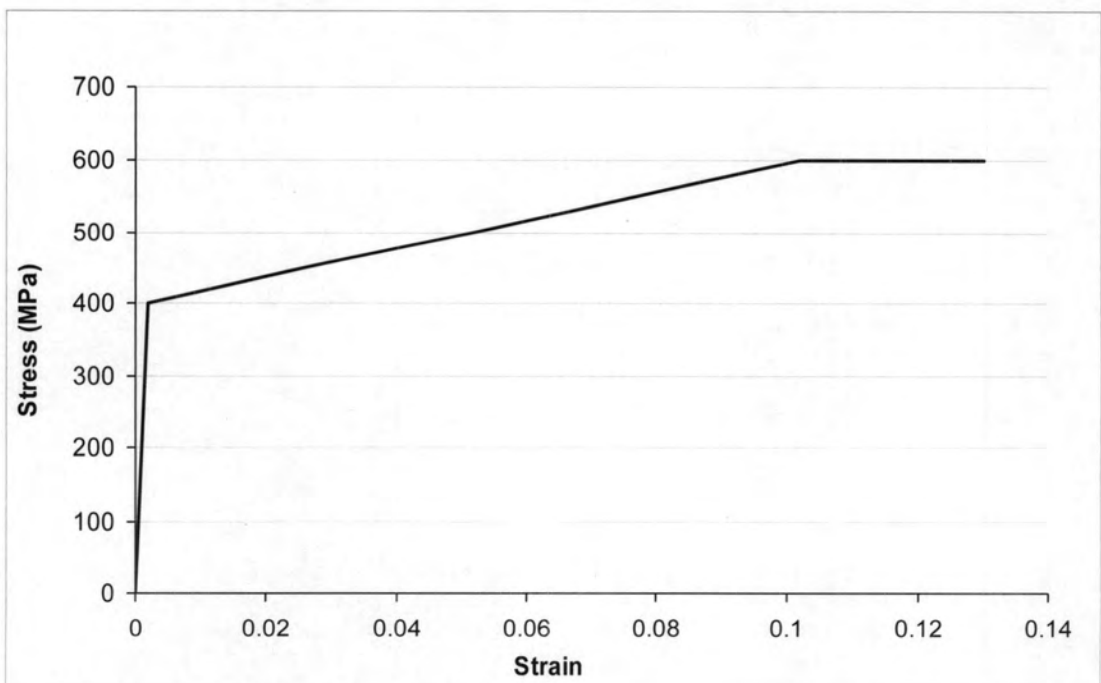
(b) Reinforcing steel

Fig. 3.6 Constitutive models employed in finite element analysis
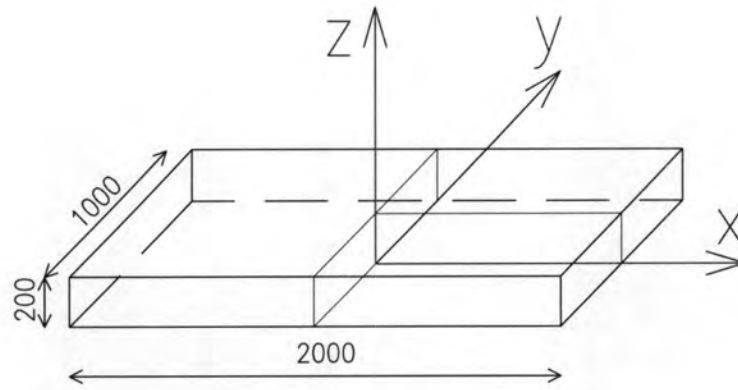
(a) Link slab coordinate system
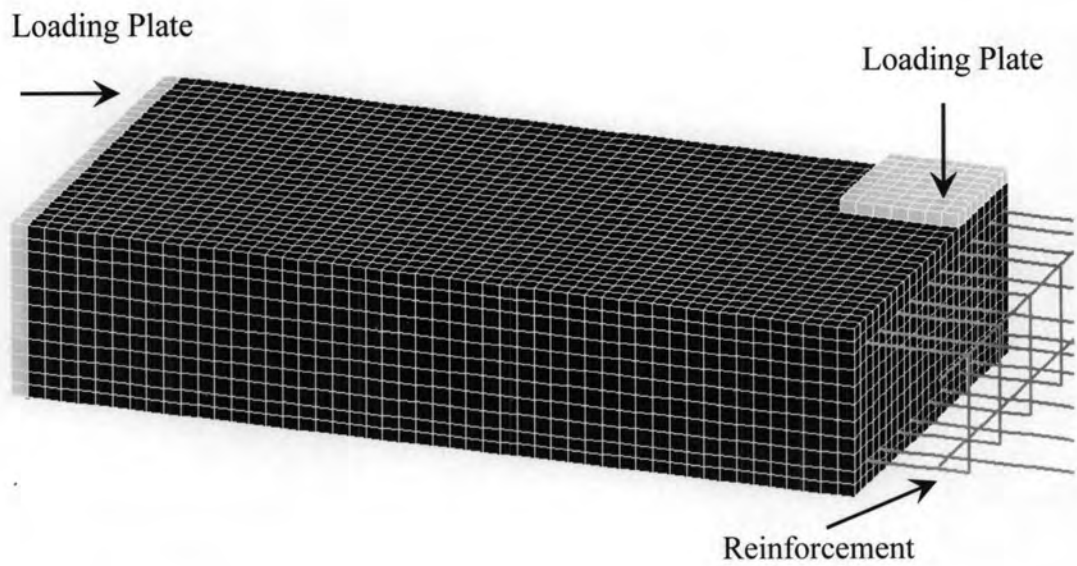
(b) Finite element discretization of link slab (quarter of specimen)

Fig. 3.7 Model of link slab
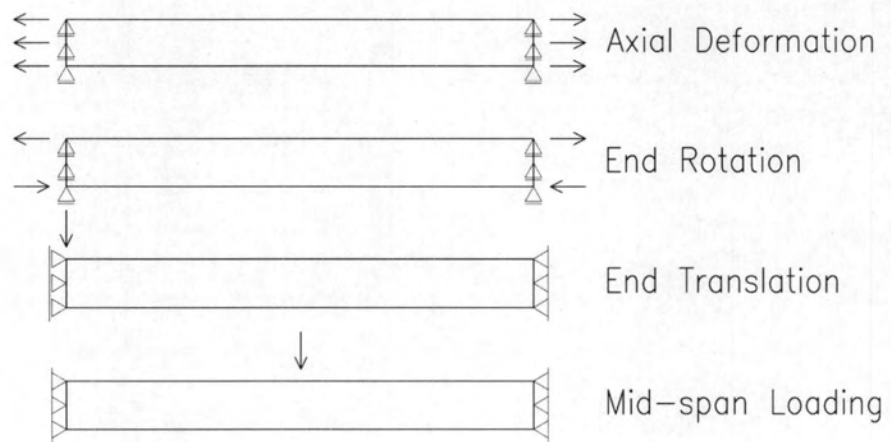
Fig. 3.8 Boundary conditions for each action
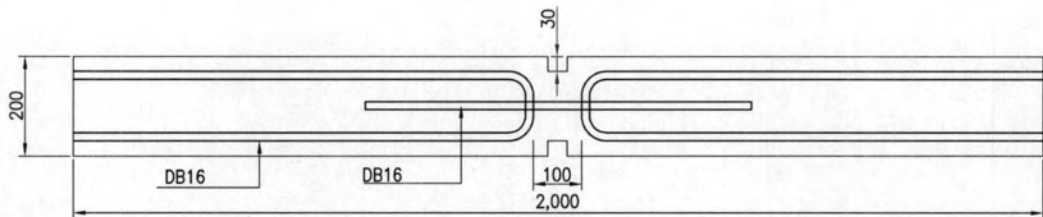
(a) Mid-span hinge (LS_H)
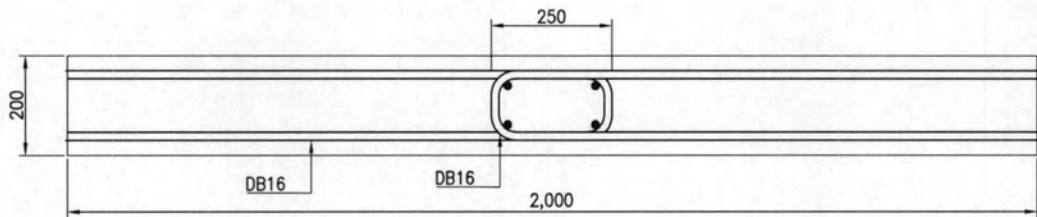
(b) Semi continuous (LS_S)
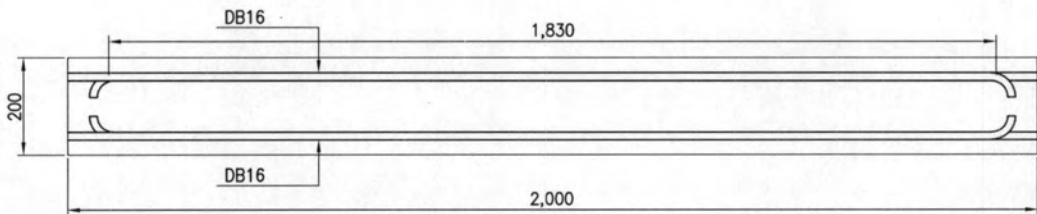
(c) Fully continuous (LS_F)

Fig. 3.9 Three types of reinforcement details
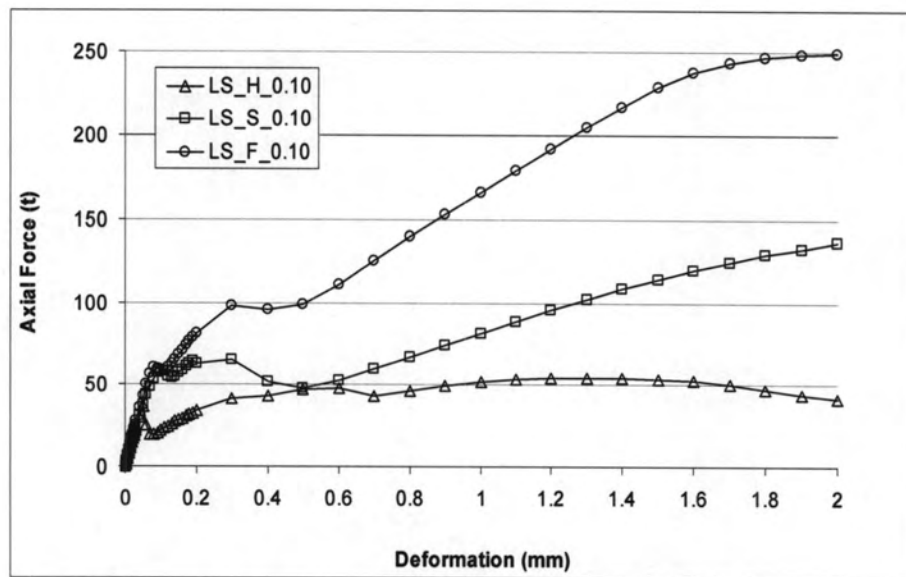
(a) Load-deformation curves
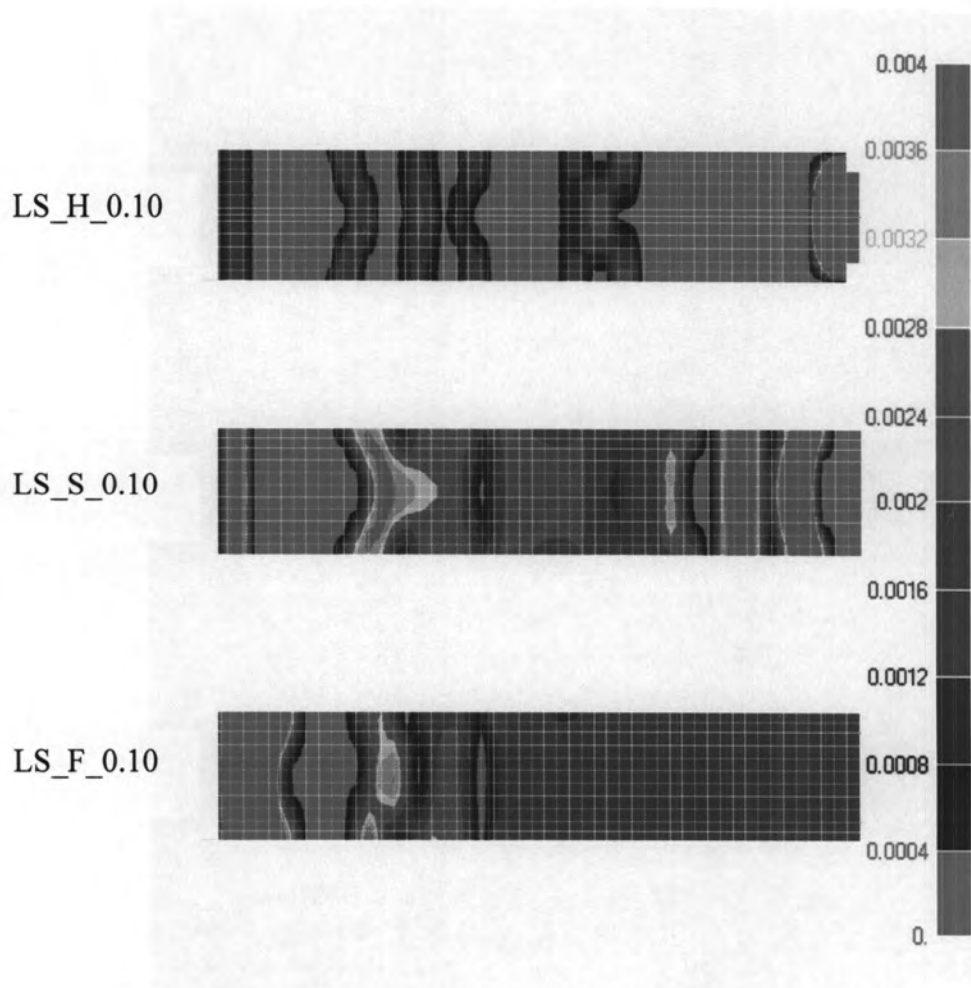
(b) Crack distribution

Fig. 3.10(a)-(b) Numerical results for axial deformation case (t/L=0.10)
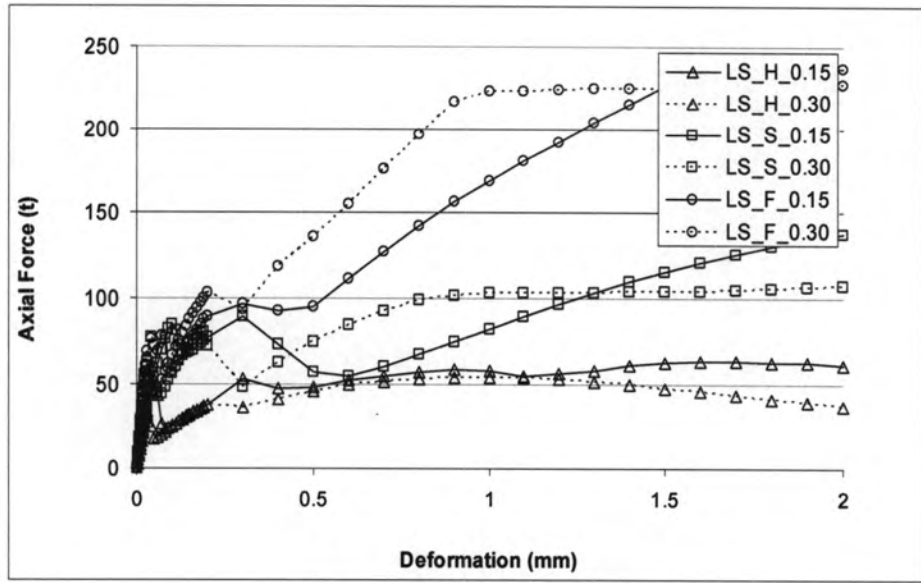
(c) Load-deformation curves
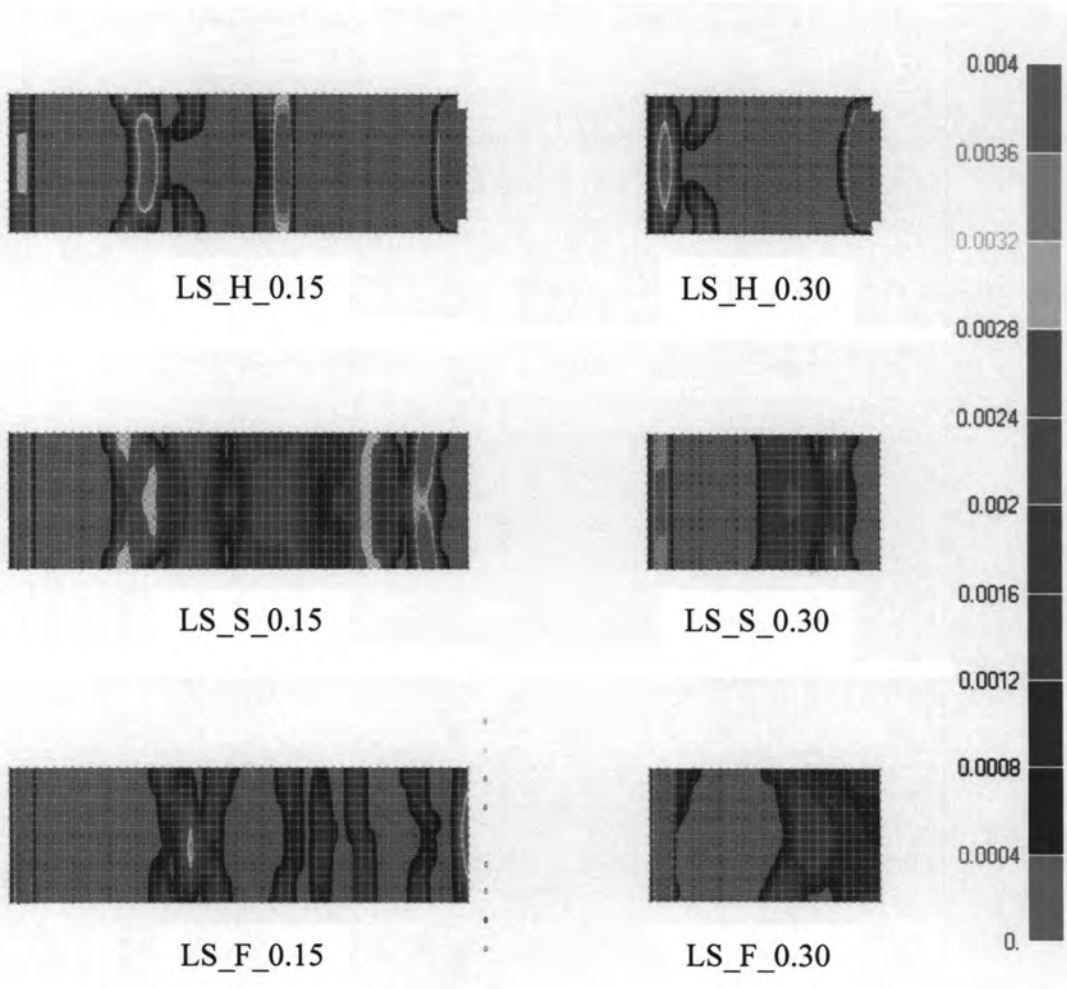
(d) Crack distribution

Fig. 3.10(c)-(d) Numerical results for axial deformation case (t/L=0.15, 0.30)
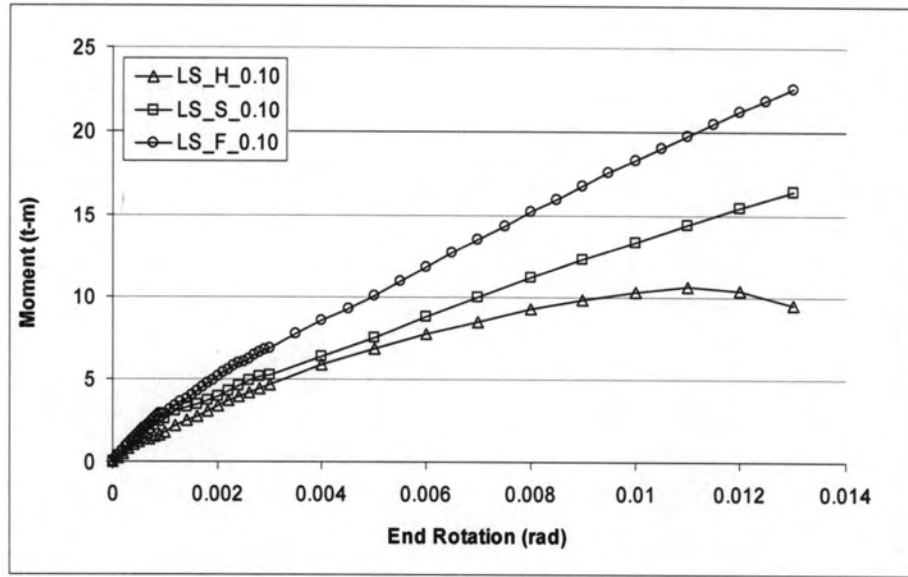
(a) Load-deformation curves
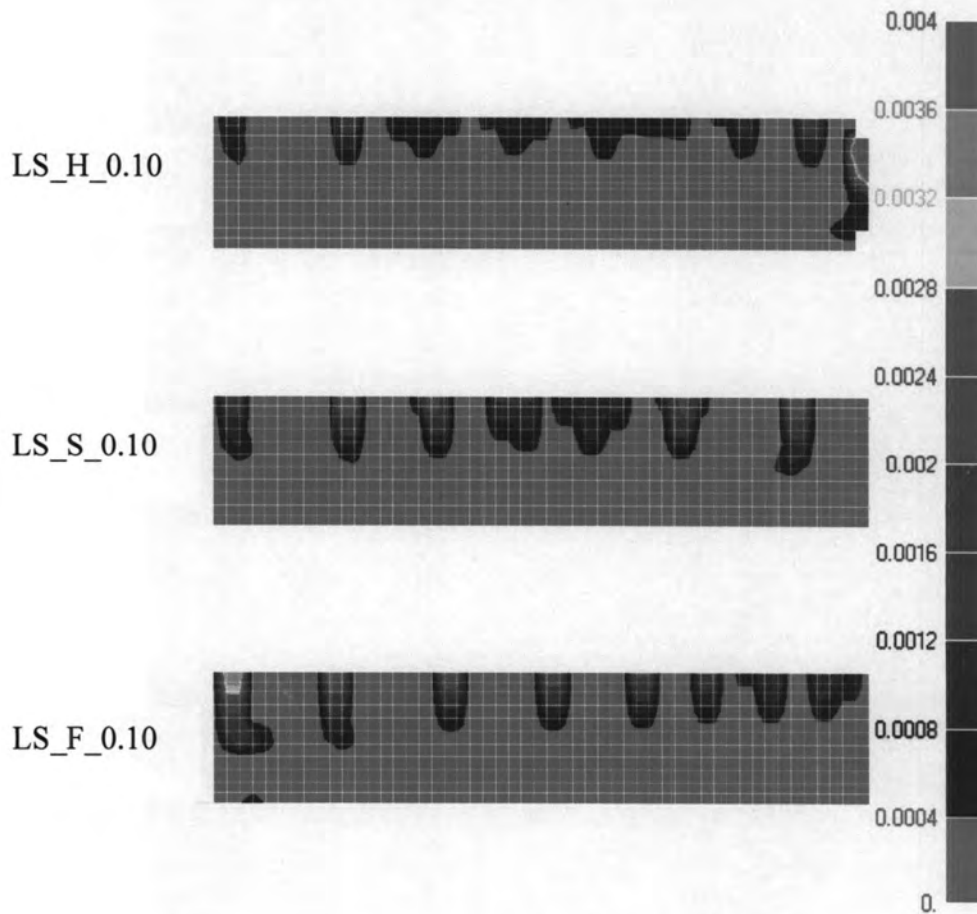
(b) Crack distribution

Fig. 3.11(a)-(b) Numerical results for end rotation case (t/L=0.10)
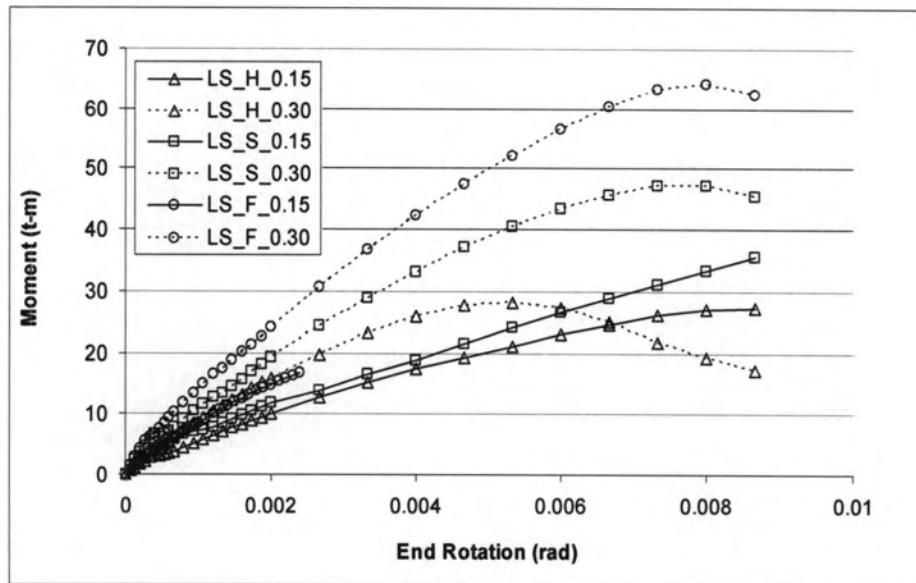
(c) Load-deformation curves
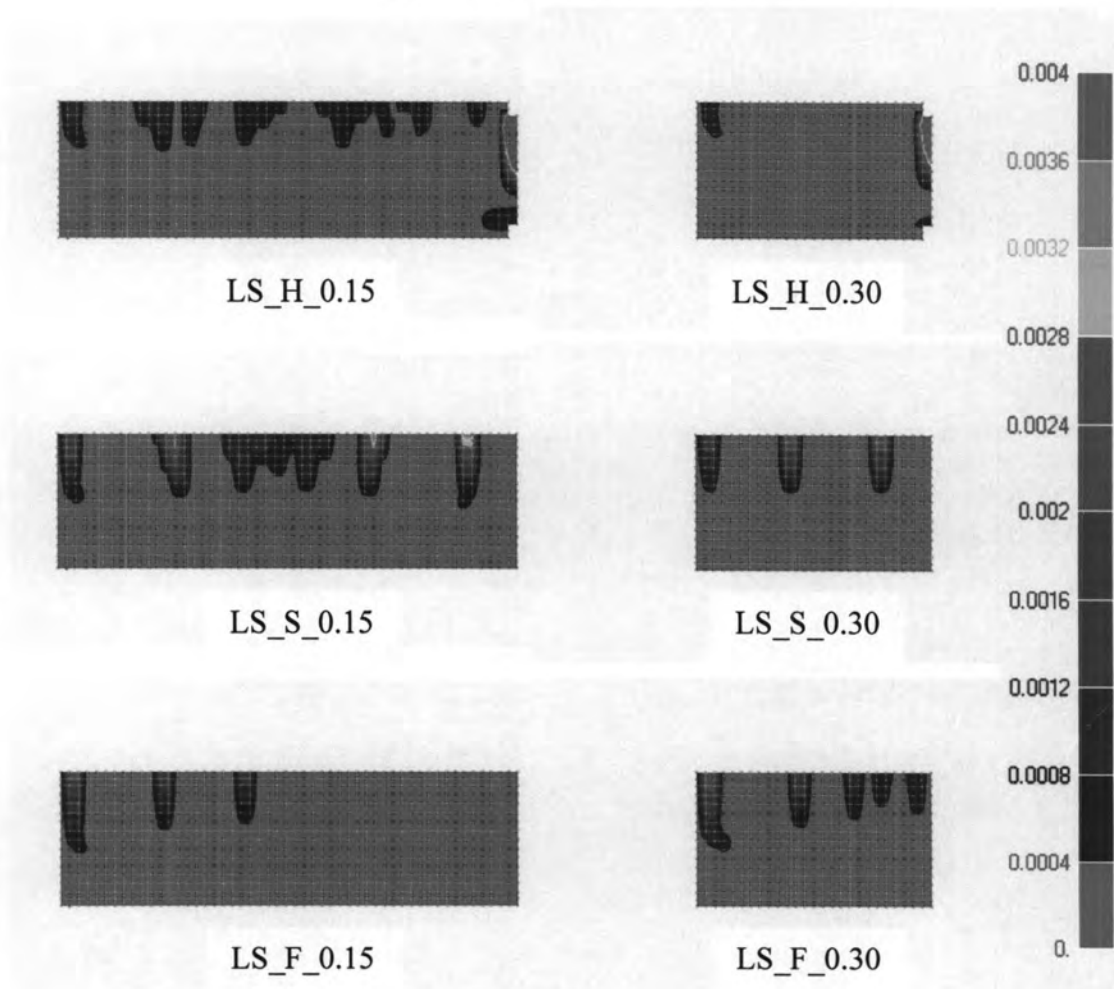
(d) Crack distribution

Fig. 3.11(c)-(d) Numerical results for end rotation case (t/L=0.15, 0.30)
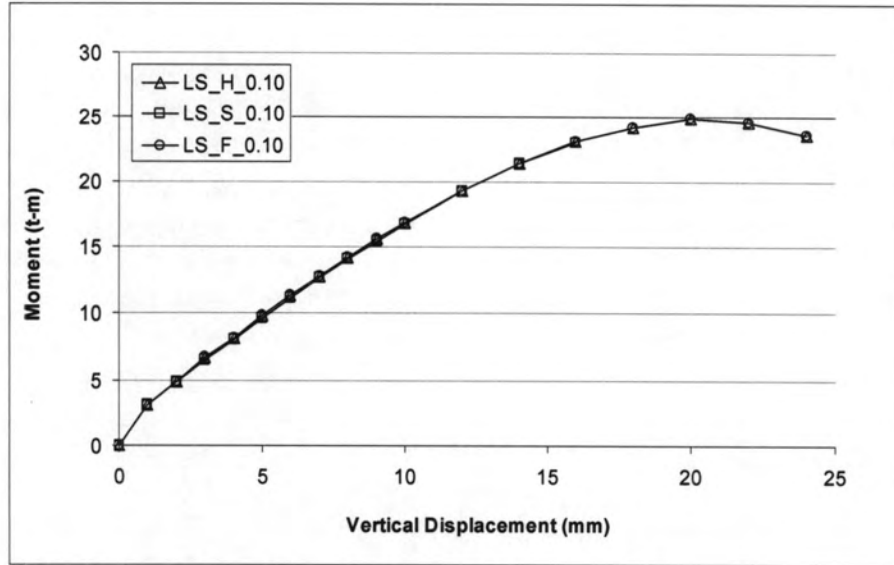
(a) Load-deformation curves
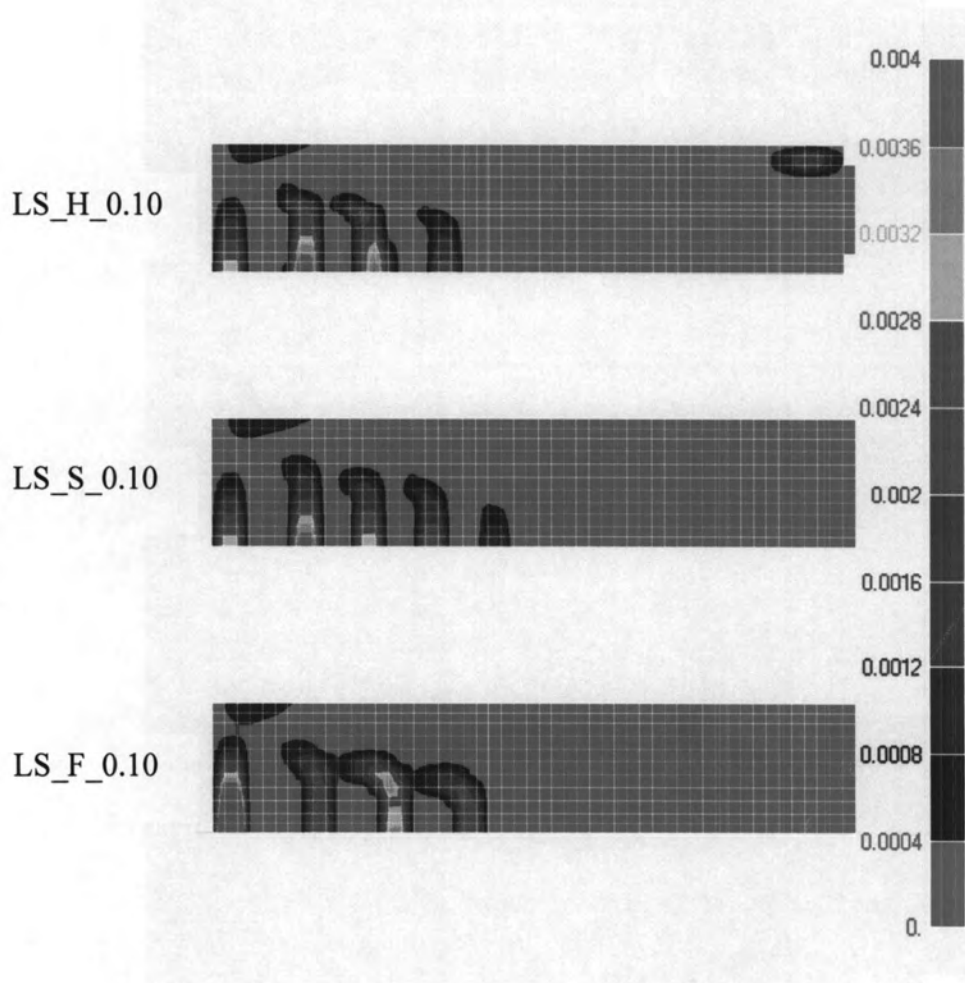
(b) Crack distribution

Fig. 3.12(a)-(b) Numerical results for end translation case (t/L=0.10)

(c) Load-deformation curves

LS_H_0.15   LS_H_0.30

LS_S_0.15   LS_S_0.30

LS_F_0.15   LS_F_0.30
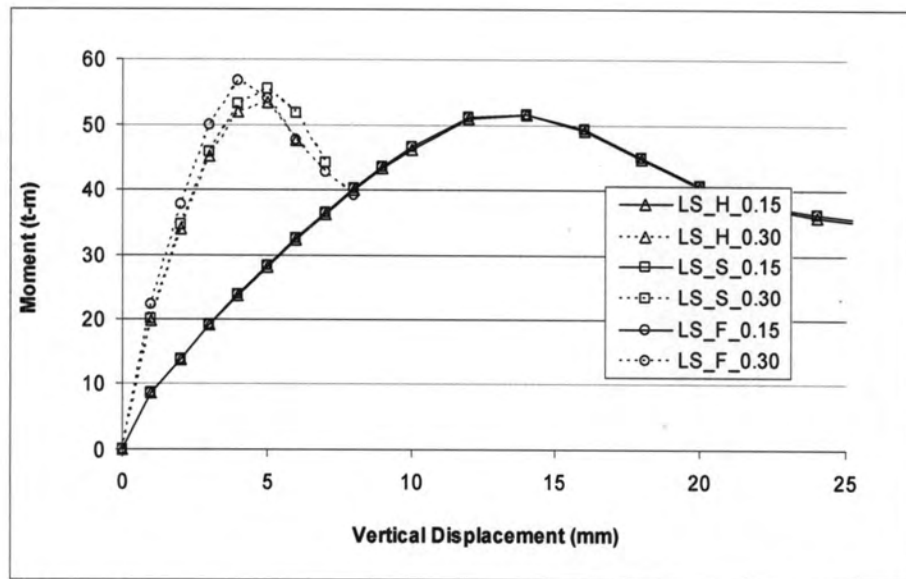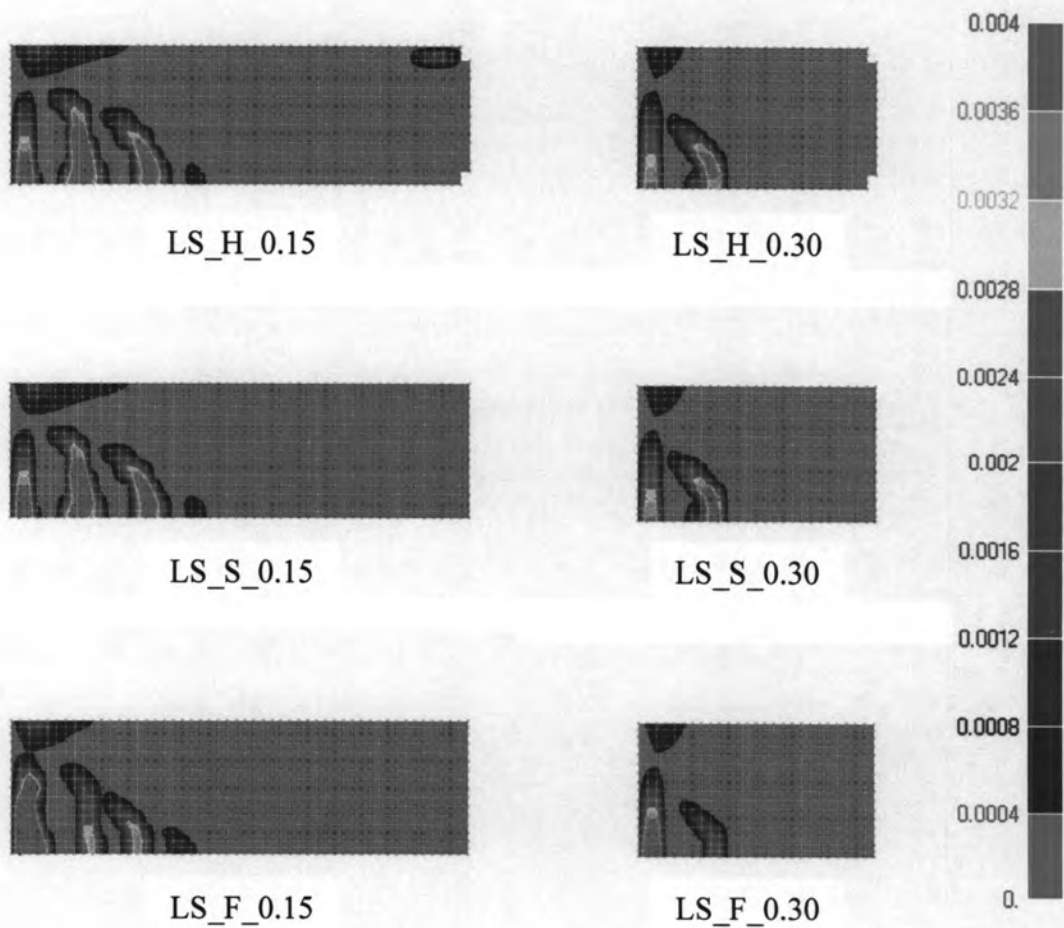
(d) Crack distribution

Fig. 3.12(c)-(d) Numerical results for end translation case (t/L=0.15, 0.30)
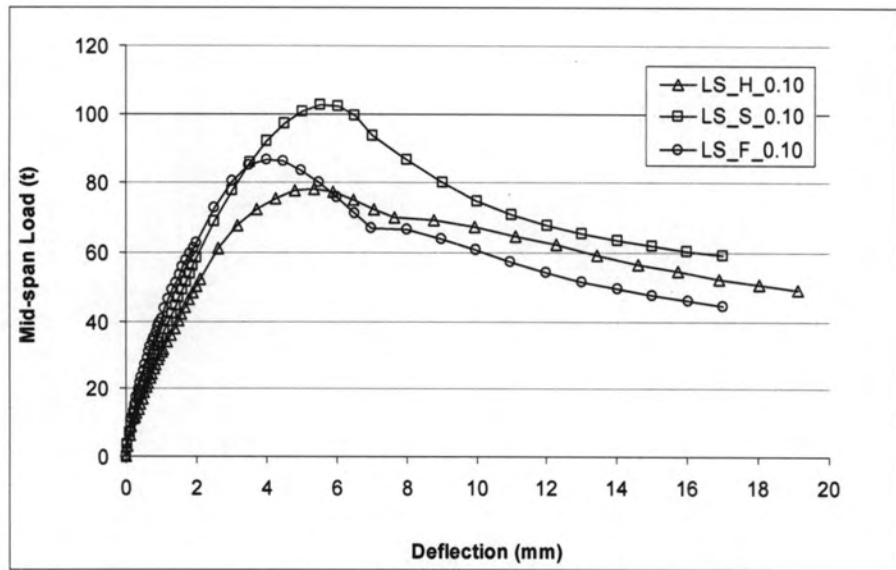
(a) Load-deformation curves
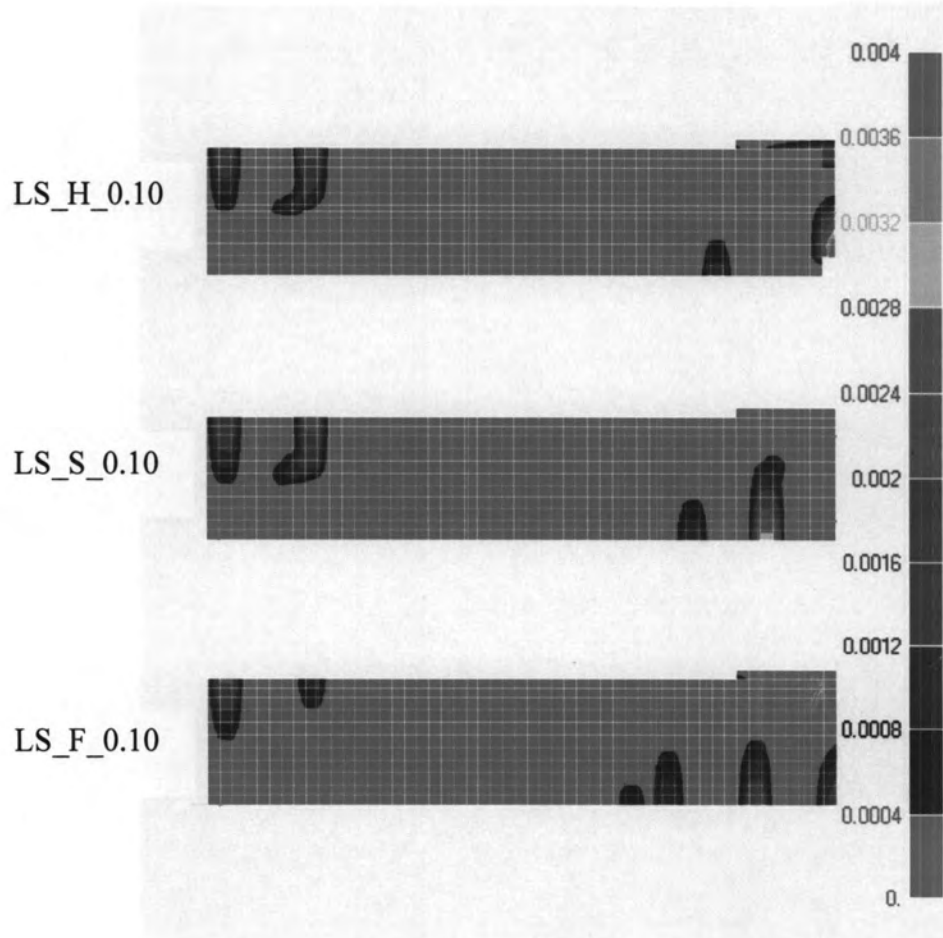
(b) Crack distribution

Fig. 3.13(a)-(b) Numerical results for mid-span loading case (t/L=0.10)
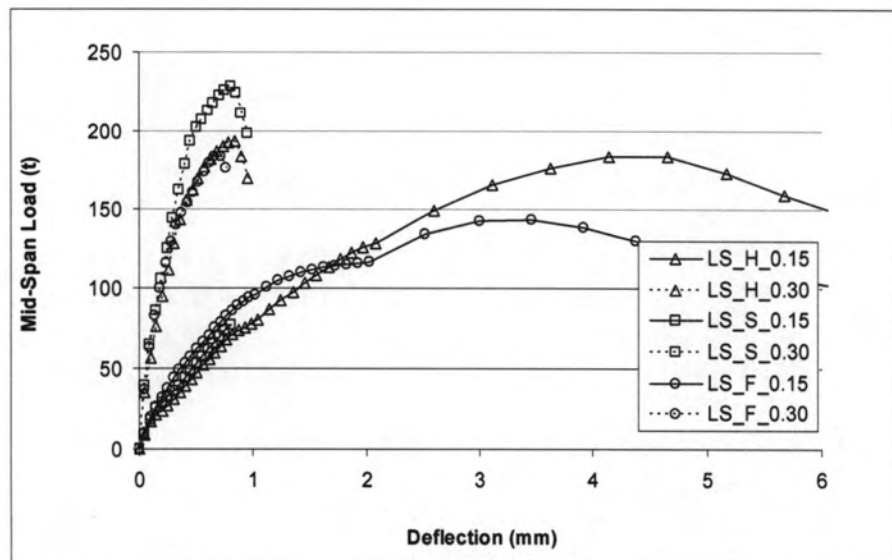
(c) Load-deformation curves
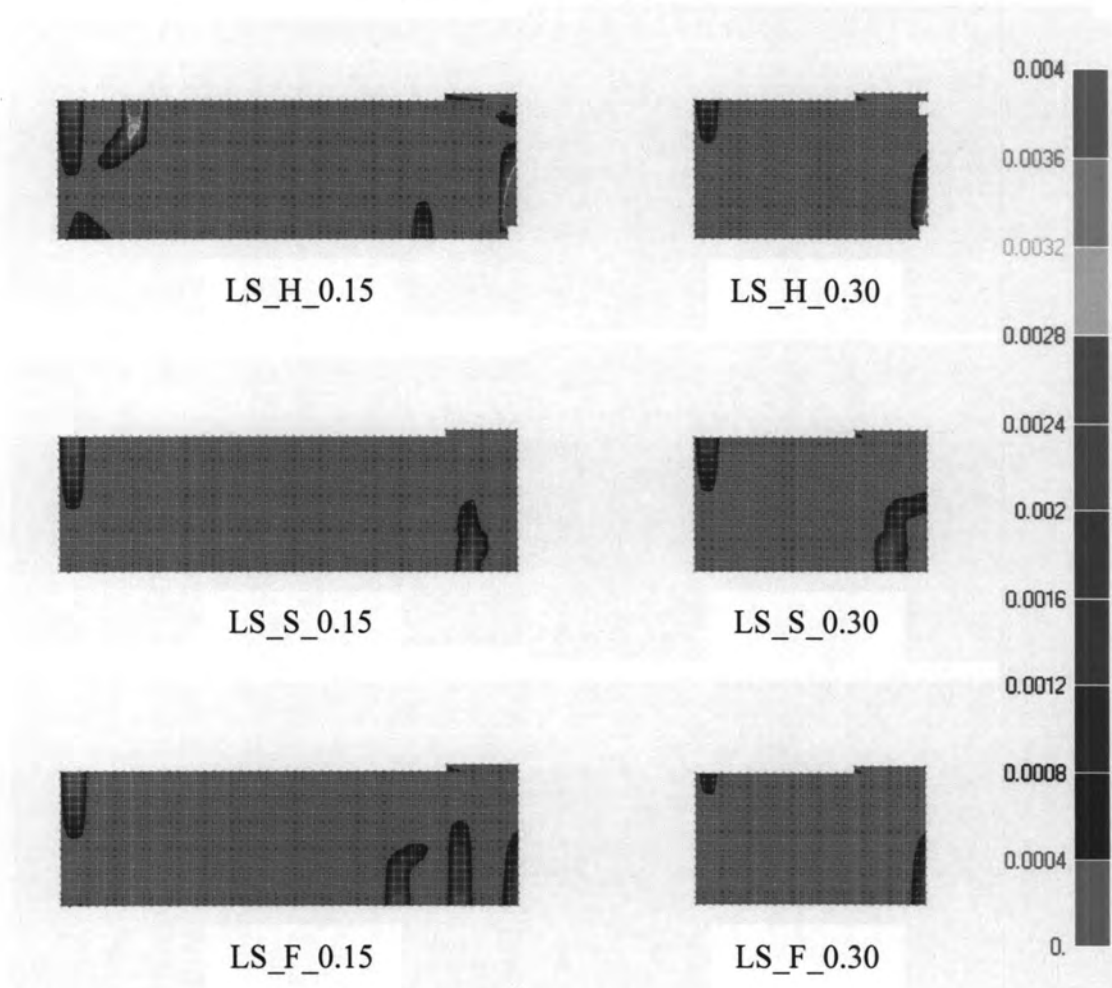
(d) Crack distribution

Fig. 3.13(c)-(d) Numerical results for mid-span loading case (t/L=0.15, 0.30)
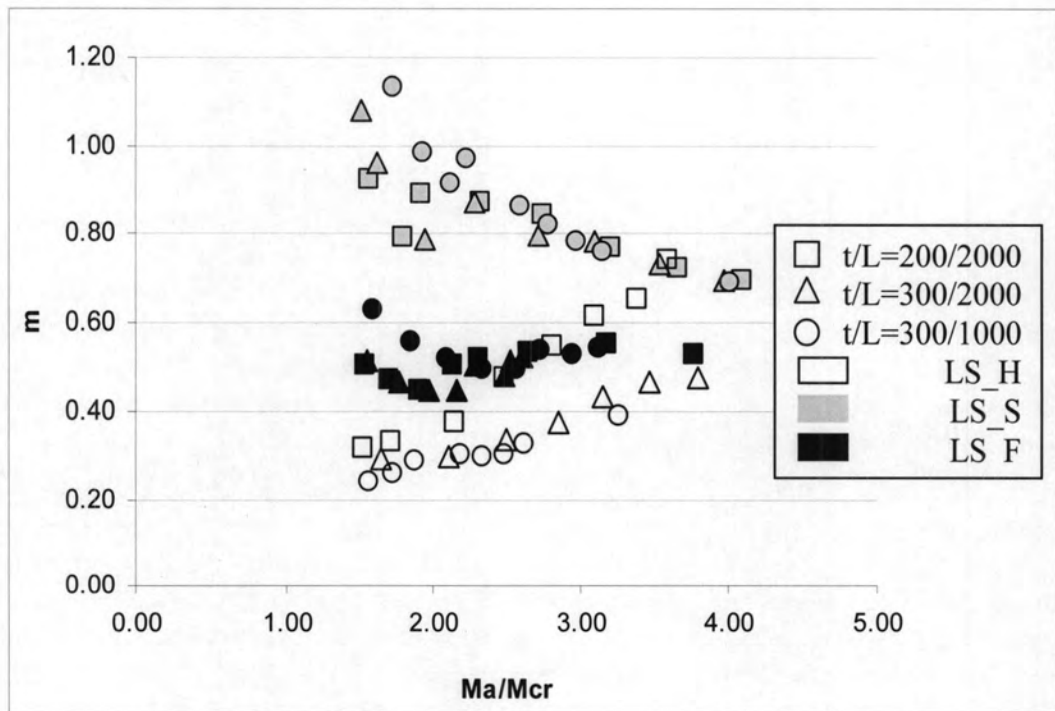
(a) End rotation
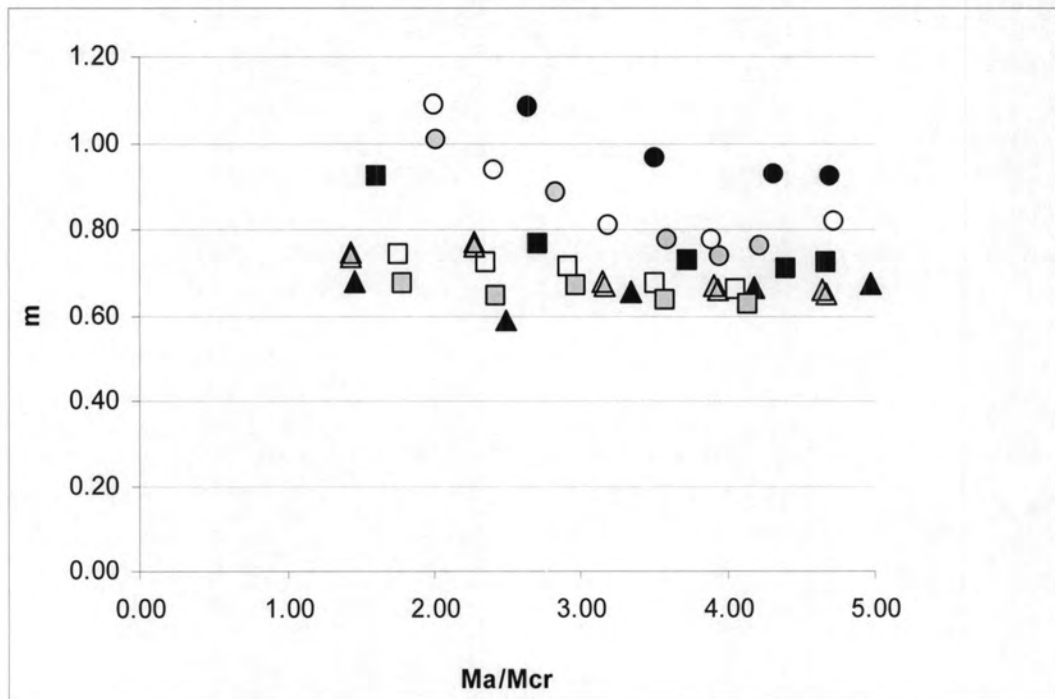
(b) End translation

Fig. 3.14 Determination of the exponent *m* (FEM)

a) Axial b) Rotation c) Translation
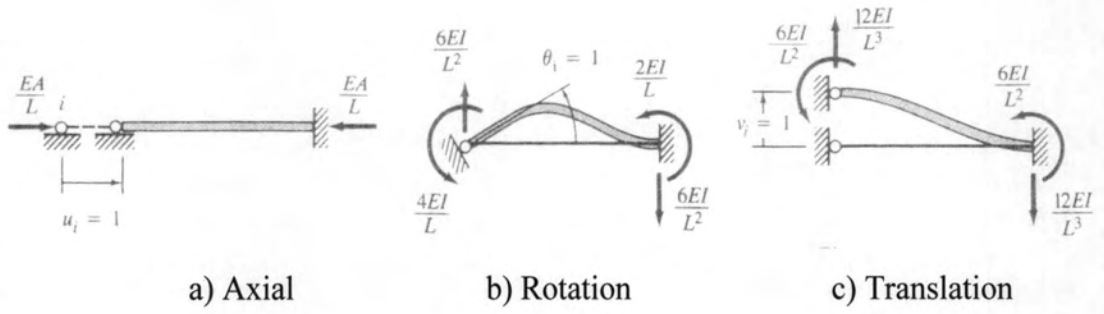
Fig. 3.15 Beam nodal forces and displacement components
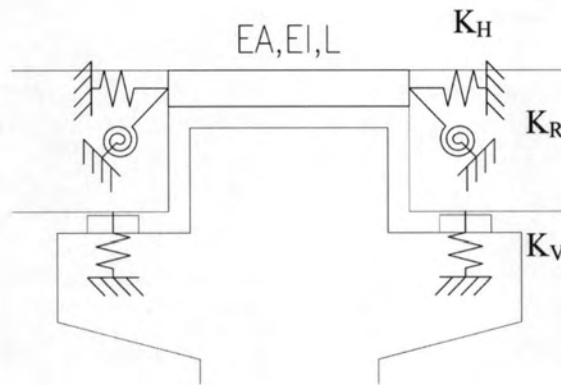
(a) Theoretical model
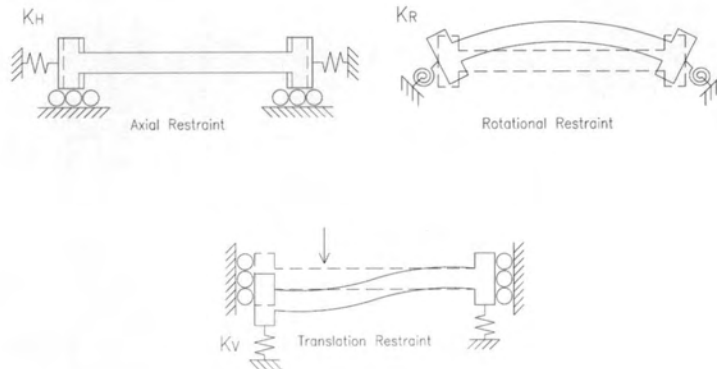
(b) Three components of restraint

Fig. 3.16 Link slab model
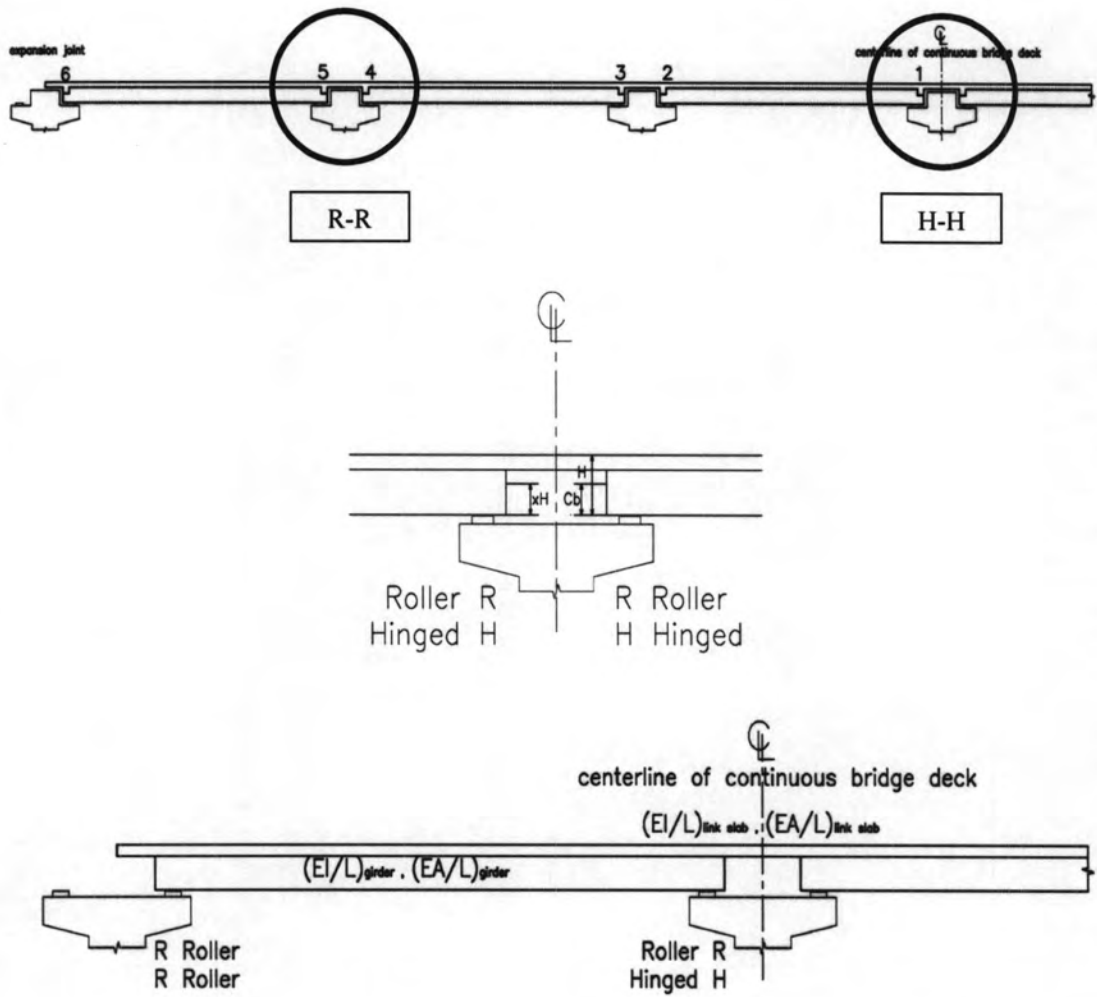
Fig. 3.17 Schematic structure and support conditions (R-R and H-H)
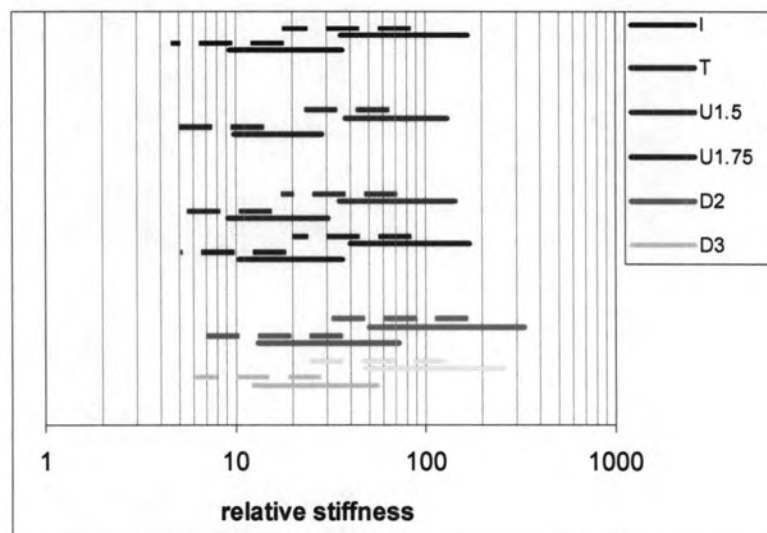
Fig. 3.18 Relative stiffness of girder and link slab
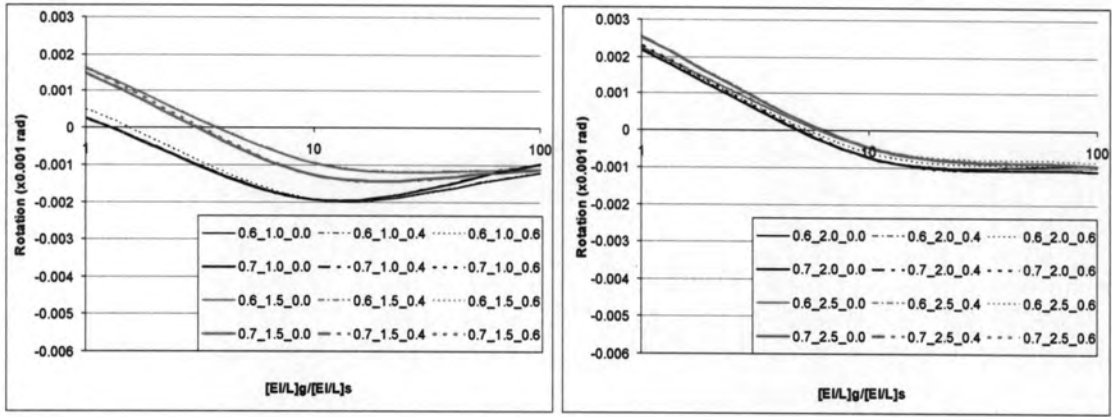
a) R-R support
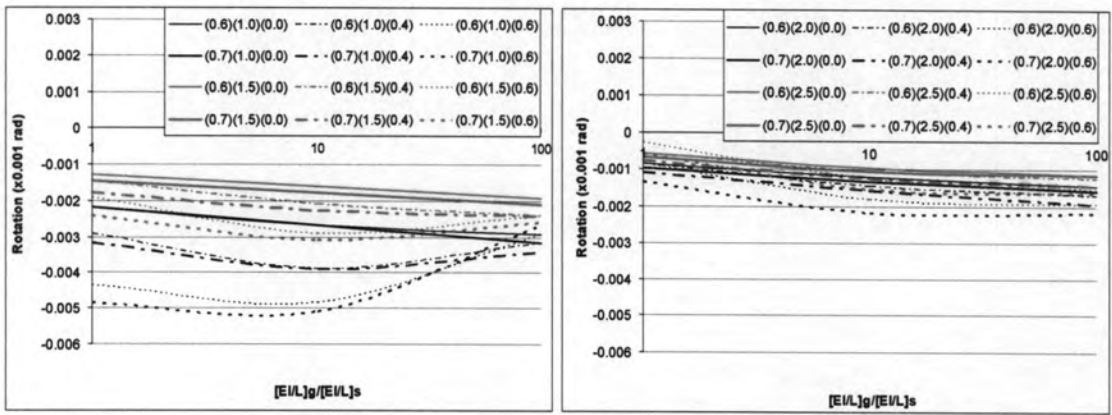
b) H-H support

Fig. 3.19(a)-(b) Rotational restraint of link slab per 1 unit elongation
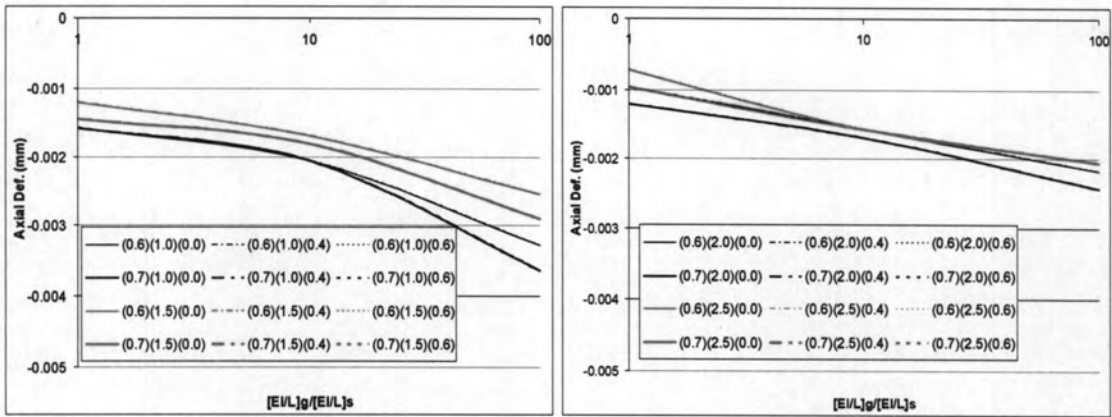
c) R-R support
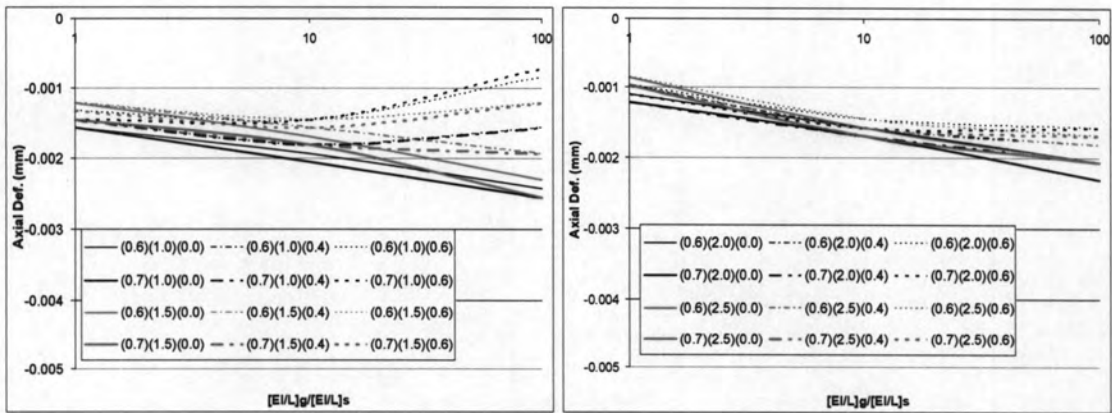
d) H-H support

Fig. 3.19(c)-(d) Axial restraint of link slab per 1 unit elongation
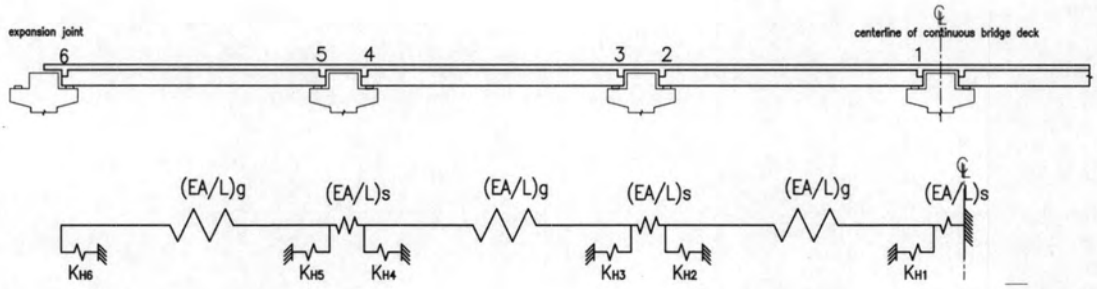
Fig. 3.20 Structural model for longitudinal movement with elastomeric bearing
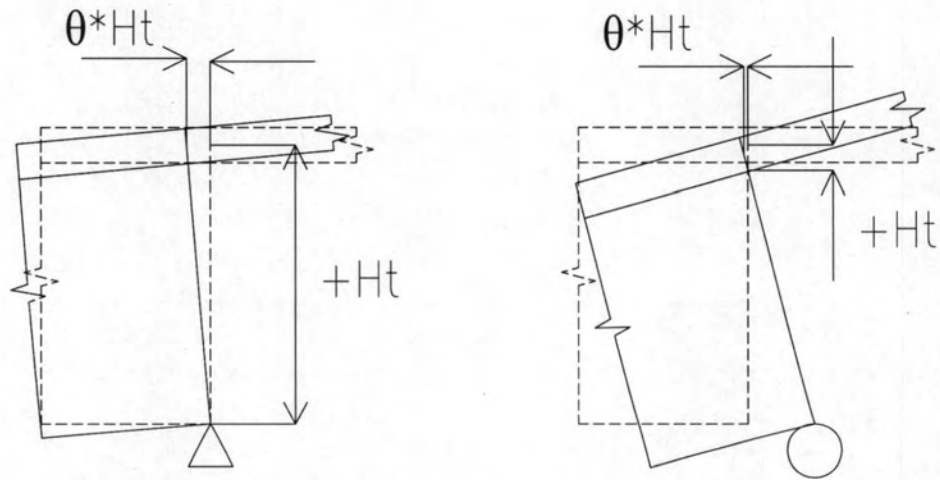
a) H-H support condition   b) R-R support condition

Fig. 3.21 Center of rotation of girder and link slab subjected to end rotation
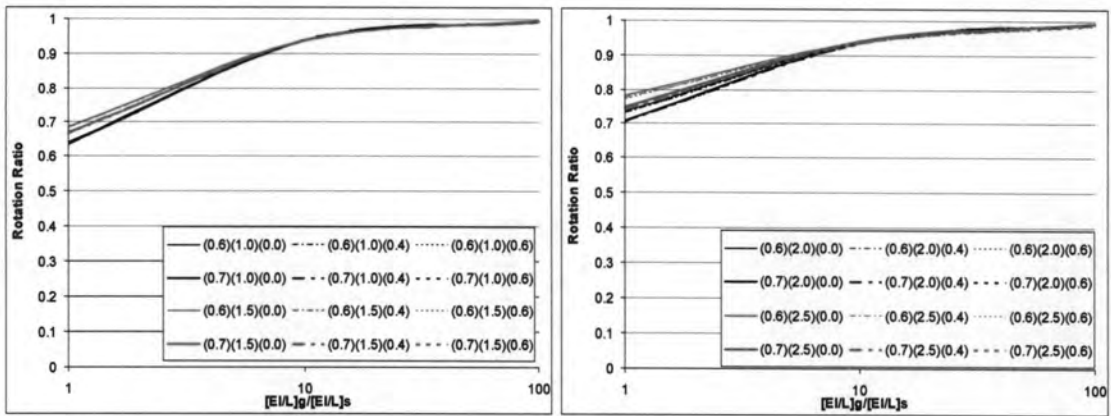
a) R-R support
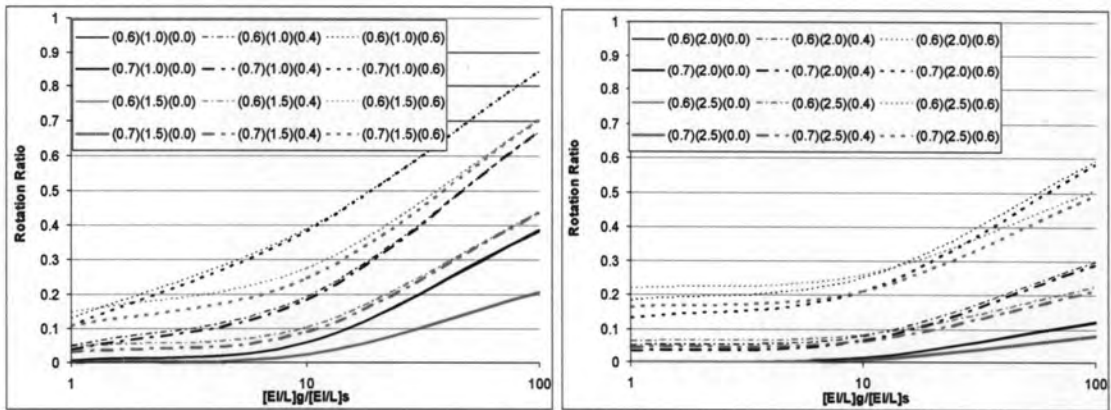
b) H-H support

Fig. 3.22(a)-(b) Rotational restraint of link slab per 1 unit end rotation
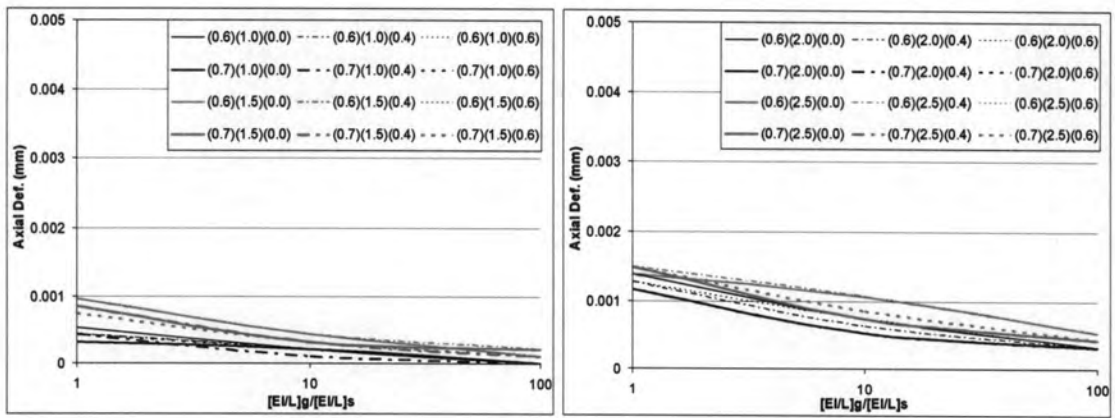
c) R-R support
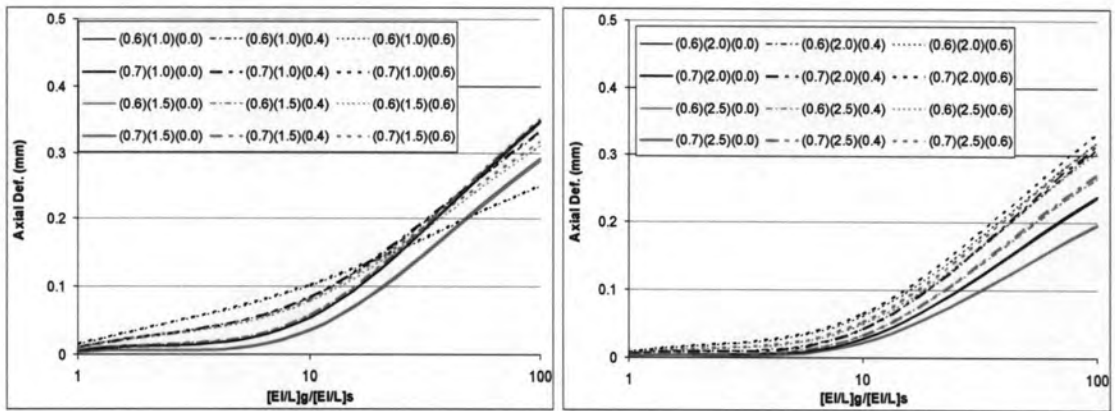
d) H-H support

Fig. 3.22(c)-(d) Axial restraint of link slab per ($\times 10^{-3}$ rad) end rotation
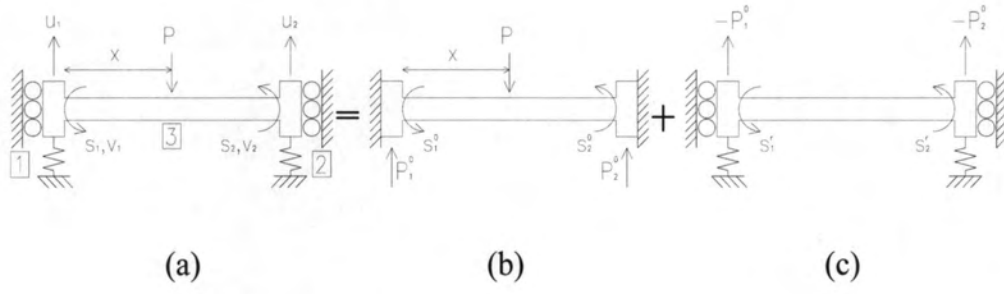
Fig. 3.23 Structural model of translational restraint
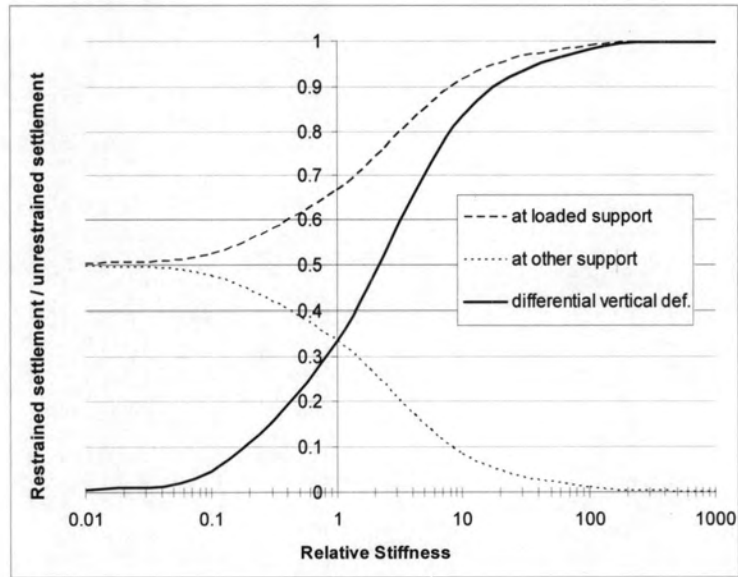
Fig. 3.24 Degree of translational restraint
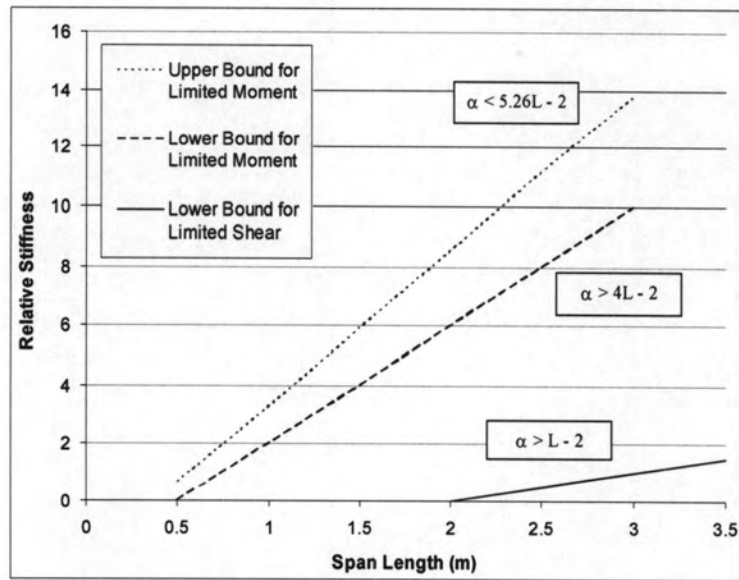
Fig. 3.25 Vertical relative stiffness to control moment and shear
for translational restraint
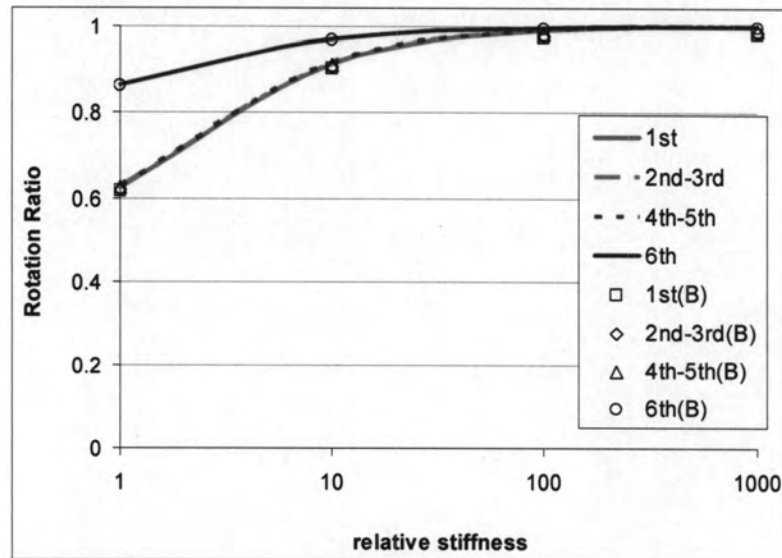
Fig. 3.26 Rotational restraint of 6-span jointless girder with R-R support and
elastomeric bearing supports
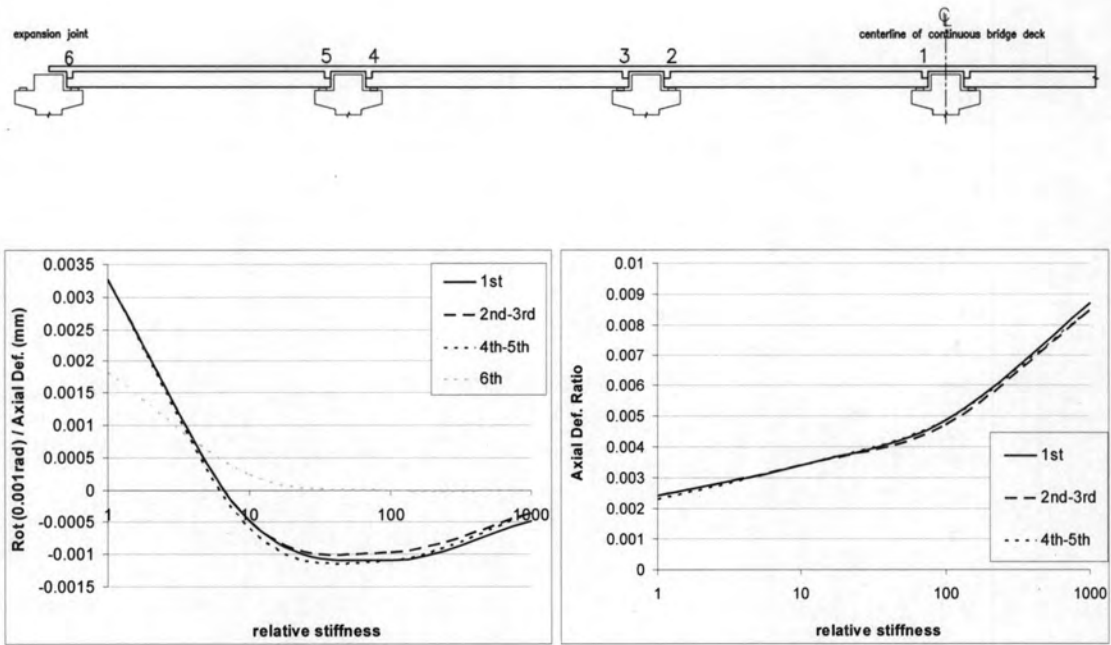
Fig. 3.27 End restraints of a 6-span jointless girder per 1 unit elongation

(roller supports)
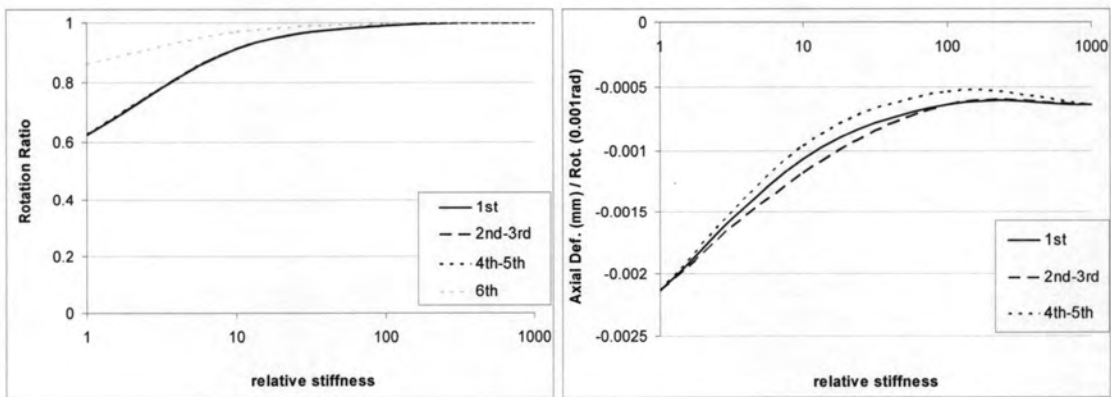
Fig. 3.28 End restraints of a 6-span jointless girder per 1 unit deflected end rotation

(roller supports)
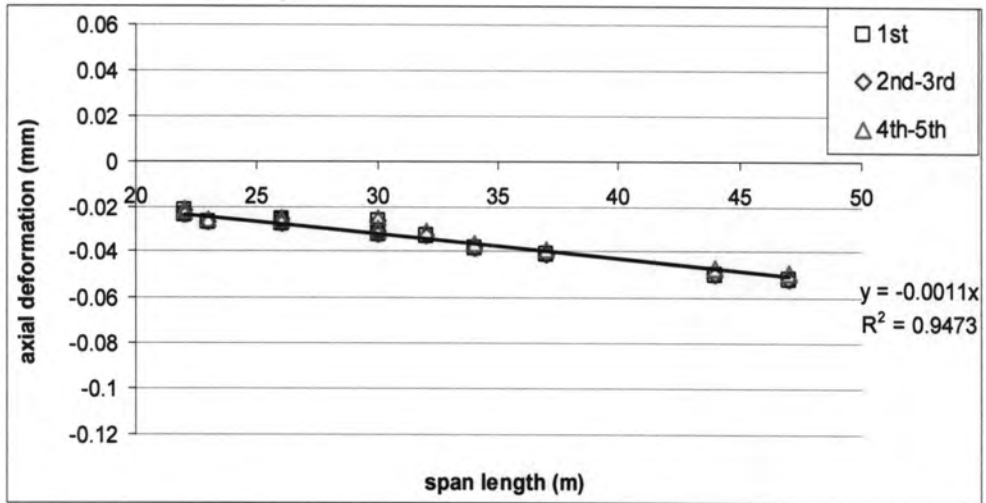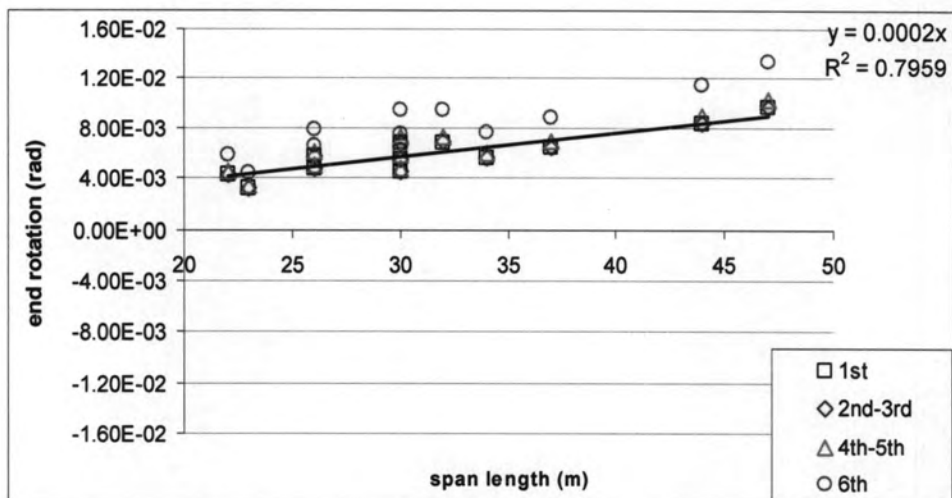
(a) relative stiffness = 1
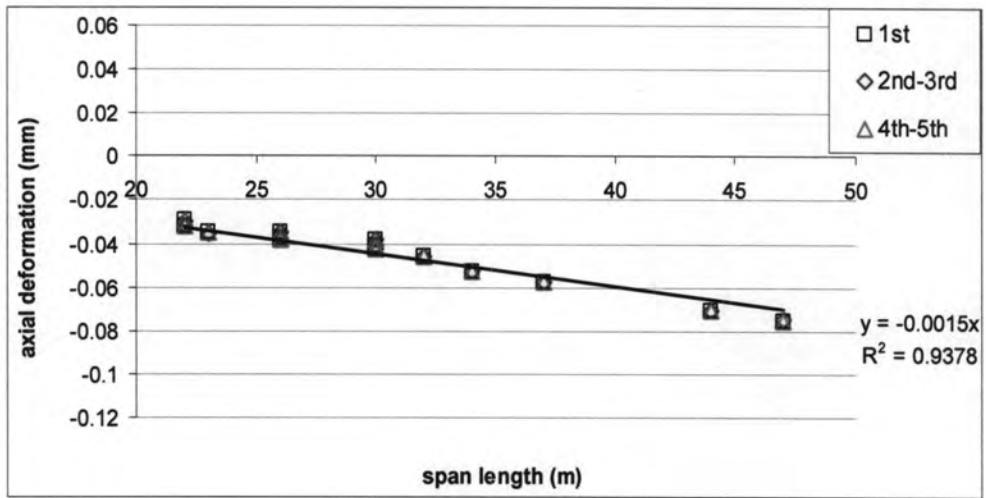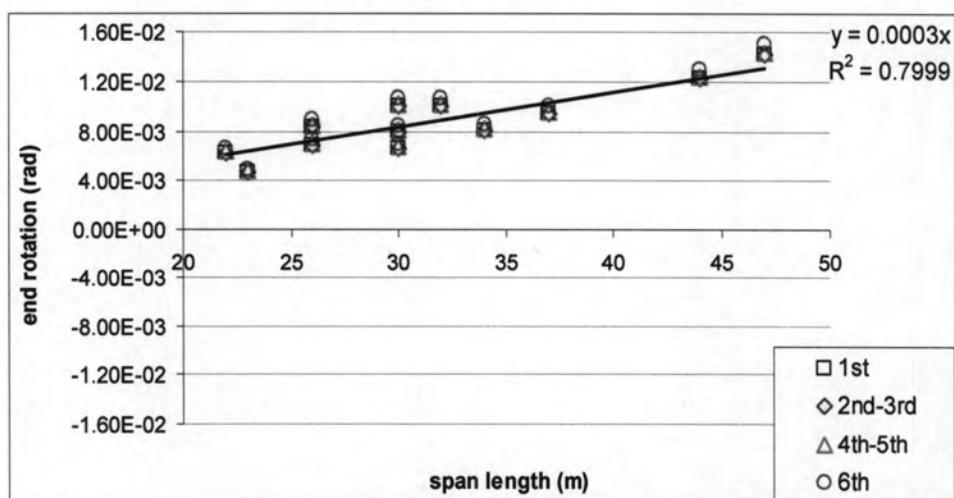

(b) relative stiffness = 10
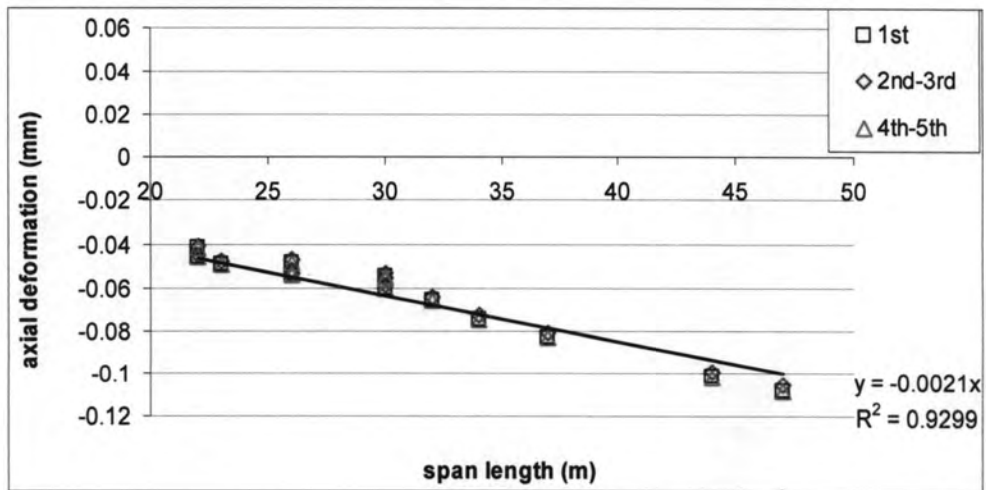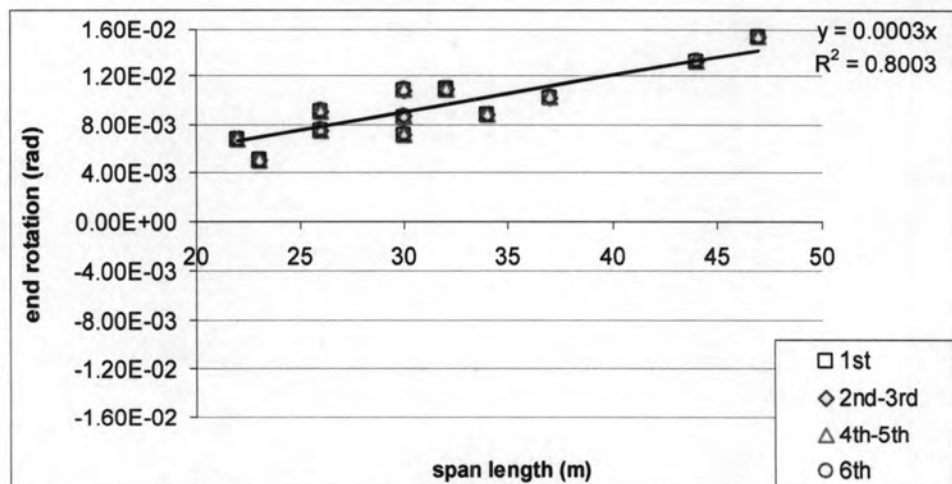

(c) relative stiffness = 100

Fig. 3.29 Axial restraint due to maximum shortening

(a) relative stiffness = 1

(b) relative stiffness = 10

(c) relative stiffness = 100

Fig. 3.30 Flexural restraint due to maximum deflected end rotation